Circulation

ORIGINAL RESEARCH ARTICLE

Splenic CD169$^+$Tim4$^+$ Marginal Metallophilic Macrophages Are Essential for Wound Healing After Myocardial Infarction

Mohamed Ameen Ismahil, PhD; Guihua Zhou, MD; Shreya Rajasekar, MS; Min Gao, PhD; Shyam S. Bansal, PhD; Bindiya Patel, PhD; Nita Limdi, PharmD, PhD, MSPH; Min Xie, MD, PhD; Sergey Antipenko, MD, PhD; Gregg Rokosh, PhD; Tariq Hamid, PhD; Sumanth D. Prabhu, MD

BACKGROUND: Fidelity of wound healing after myocardial infarction (MI) is an important determinant of subsequent adverse cardiac remodeling and failure. Macrophages derived from infiltrating Ly6C^{hi} (lymphocyte antigen 6 complex, locus C) blood monocytes are a key component of this healing response; however, the importance of other macrophage populations is unclear.

METHODS: We used a variety of in vivo murine models and orthogonal approaches, including surgical MI, flow cytometry and single-cell RNA sequencing, lineage tracing and cell tracking, splenectomy, parabiosis, cell adoptive transfer, and functional characterization, to establish an essential role for splenic CD169$^+$Tim4$^+$ (cluster of differentiation 169$^+$; T cell immunoglobulin– and mucin-domain–containing molecule 4) marginal metallophilic macrophages (MMMs) in post-MI wound healing in mice. Flow cytometry was used to measure circulating CD169$^+$Tim4$^+$ monocytes in humans with ST-segment–elevation MI and control participants with stable coronary artery disease undergoing elective percutaneous coronary intervention.

RESULTS: Splenic CD169$^+$Tim4$^+$ MMMs circulate in blood as Ly6C^{low} monocytes expressing macrophage markers and help populate CD169$^+$Tim4$^+$CCR2$^-$LYVE1^{low} macrophages in the naive heart. After acute MI, splenic MMMs augment phagocytosis and CCR (C-C motif chemokine receptor) 3 and CCR4 expression, and robustly mobilize to the heart, resulting in marked expansion of cardiac CD169$^+$Tim4$^+$LYVE1^{low} macrophages with an immunomodulatory and proresolving gene signature. These macrophages are obligatory for apoptotic neutrophil clearance, suppression of inflammation, and induction of a reparative macrophage phenotype in the infarcted heart. Splenic MMMs are both necessary and sufficient for post-MI wound healing, and limit late pathological remodeling. Liver X receptor-α agonist–induced expansion of the splenic marginal zone and MMMs during acute MI alleviates inflammation and improves short- and long-term cardiac remodeling. Humans with acute ST-segment–elevation MI also exhibit expansion of circulating CD169$^+$Tim4$^+$ cells, primarily within the intermediate (CD14$^+$CD16$^+$) monocyte population.

CONCLUSIONS: Splenic CD169$^+$Tim4$^+$ MMMs are required for proresolving and reparative responses after MI and can be manipulated for therapeutic benefit to limit long-term heart failure.

Key Words: heart failure ■ inflammation ■ macrophages ■ myocardial infarction ■ spleen

Editorial, see p 1748

Correspondence to: Sumanth D. Prabhu, MD, Division of Cardiology, Washington University in St Louis, 660 S Euclid Ave, MSC 8086-43-13, St Louis, MO 63110. Email prabhu@wustl.edu

Supplemental Material is available at https://www.ahajournals.org/doi/suppl/10.1161/CIRCULATIONAHA.124.071772.
For Sources of Funding and Disclosures, see page 1727.

Circulation is available at www.ahajournals.org/journal/circ

Clinical Perspective

What Is New?

- We establish for the first time that metallophilic marginal macrophages from the spleen, expressing the markers cluster of differentiation (CD) 169 and T cell immunoglobulin– and mucin-domain–containing molecule 4 (Tim4), circulate in blood as Ly6C^{low} (lymphocyte antigen 6 complex, locus C) monocytes expressing macrophage markers and traffic to the heart to help maintain the CD169^{+}Tim4^{+}CCR2^{-}LYVE1^{low} macrophage population in the heart.
- After acute myocardial infarction, splenic metallophilic marginal macrophages augment cardiac trafficking in response to chemotactic signals, resulting in expansion of CD169^{+}Tim4^{+} macrophages in the heart that play an essential role in post–myocardial infarction (MI) efferocytosis, wound healing, and repair, while limiting longer-term adverse cardiac remodeling.
- Analogous to mice, humans also exhibit circulating CD169^{+}Tim4^{+} cells, primarily within the intermediate (CD14^{+}CD16^{+}) blood monocyte population, which expand after acute ST-segment–elevation MI.

What Are the Clinical Implications?

- This study highlights the importance of the cardiosplenic axis in acute MI, and the splenic marginal zone, in determining the course and outcome of post-MI left ventricular remodeling.
- Pharmacological expansion of splenic marginal zone macrophages alleviated post-MI adverse left ventricular remodeling and inflammation, suggesting that splenic modulation is a potential translational therapeutic approach for limiting post-MI inflammation and improving heart repair.

Nonstandard Abbreviations and Acronyms

7-AAD	7-aminoactinomycin D
ARRIVE	Animal Research: Reporting of In Vivo Experiments
CCL	C-C chemokine ligand
CCR	C-C motif chemokine receptor
CD	cluster of differentiation
C-FLIP	cellular FLICE-like inhibitory protein
CX3CR1	C-X3-C motif chemokine receptor 1
DC	dendritic cell
DEG	differentially expressed gene
DT	diphtheria toxin
DTR	diphtheria toxin receptor
EDV	end-diastolic volume
EF	ejection fraction
ESV	end-systolic volume
FACS	fluorescence-activated cell sorting
G-CSF	granulocyte colony-stimulating factor
GFP	green fluorescent protein
HF	heart failure
HLA-DR	human leukocyte antigen–DR
ICAM-1	intercellular adhesion molecule 1
IL	interleukin
iNOS	inducible nitric oxide synthase
LV	left ventricular
LXRα	liver X receptor α
Ly6C	lymphocyte antigen 6 complex, locus C
LYVE1	lymphatic vessel endothelial hyaluronan receptor 1
MaFIA	macrophage Fas-induced apoptosis
MHC II	major histocompatibility complex class II
MI	myocardial infarction
MMM	metallophilic marginal macrophage
MZ	marginal zone
MZM	marginal zone macrophage
NR4A1	nuclear receptor subfamily 4 group a member 1
PCI	percutaneous coronary intervention
RNA-seq	RNA sequencing
STEMI	ST-segment–elevation myocardial infarction
Tim4	T cell immunoglobulin– and mucin-domain–containing molecule 4
WT	wild-type

Myocardial infarction (MI) triggers an orchestrated wound-healing response initially comprising intense inflammation and clearance of dead cells, followed by inflammation resolution, wound healing, and scar formation.[1] Whereas this biphasic response is required for effective tissue repair, an inflammatory response that is excessively vigorous or fails to resolve in a timely manner can lead to deleterious left ventricular (LV) remodeling and heart failure (HF).[1] Innate immune cells are crucial to this process. The inflammatory phase is dominated early by infiltrating neutrophils, and subsequently by Ly6C^{hi}CX3CR1^{low} (lymphocyte antigen 6 complex, locus C; C-X3-C motif chemokine receptor 1) monocytes derived from the spleen and bone marrow, as well as proinflammatory macrophages.[2–5] In the healing phase, reparative Ly6C^{low} macrophages are generated locally and proliferate in the heart. These cells are also derived from the initial surge of Ly6C^{hi} monocytes, through a process dependent on the nuclear hormone receptor Nr4a1 (nuclear receptor subfamily 4 group a member 1).[2] The specific triggers responsible for the switch from proinflammatory to reparative cells in the infarcted heart are not fully defined, but may relate to the phagocytic clearance of dead cells, including apoptotic cardiomyocytes

and neutrophils,[6,7] which induces a proresolving phenotype in macrophages.[1]

Whereas the role of Ly6C^{hi} monocytes and Ly6C^{hi} monocyte-derived macrophages after MI has been well-delineated, the importance of other macrophage populations remains unclear. The subcapsular red pulp of the spleen is an important reservoir of Ly6C^{hi} monocytes that mobilize to the infarcted heart.[3,4,8] However, beyond the red pulp, the spleen contains several macrophage populations with specialized functions. Prominent among these are macrophages in the marginal zone (MZ) that surrounds the splenic white pulp.[9,10] The MZ is an important watershed between lymphoid tissue and blood, characterized by continuous leukocyte transit. Along with SIGN-R1^{+}MARCO^{+} MZ macrophages (MZMs), the mouse MZ harbors cluster of differentiation (CD) 169 (sialoadhesin)$^{+}$ marginal metallophilic macrophages (MMMs), which play crucial roles in antigen capture and processing; communication with dendritic cells, T cells, and B cells; regulation of apoptotic cell clearance; and facilitation of immune tolerance.[9–11] CD169^{+} MMMs coordinate host immune responses that affect both inflammation and immunoregulation.[12]

The phosphatidylserine receptor T cell immunoglobulin– and mucin-domain–containing molecule 4 (Tim4) allows for the recognition and phagocytosis of apoptotic cells,[13] and, along with LYVE1 (lymphatic vessel endothelial hyaluronan receptor 1), has been proposed as a specific marker of resident tissue macrophages.[14,15] Tim4 further identifies an important tissue CD169^{+} macrophage subset capable of suppressing local immune responses.[16] As proper healing after MI necessitates both inflammation resolution and efficient apoptotic cell clearance, we posited that CD169^{+}Tim4^{+} MMMs from the spleen may play a central role in these events. However, whether splenic CD169^{+}Tim4^{+} MMMs mobilize to the heart during acute MI is unknown. Moreover, the pathophysiological role of splenic MMMs in post-MI repair, and the subsequent development of adverse LV remodeling and HF, is unexplored. Therefore, we tested the hypothesis that splenic CD169^{+}Tim4^{+} MMMs infiltrate the acutely infarcted heart and play an essential role in inflammation resolution and wound healing after MI.

METHODS

Full Methods are presented in the Supplemental Material.

Data Availability Statement

Data, analytical methods, and study materials will be made available to other researchers upon reasonable request after ensuring compliance with applicable legal guidelines. RNA sequencing (RNA-seq) data are accessible in the Gene Expression Omnibus (accession number GSE210798 for bulk RNA-seq and GSE289921 for single-cell RNA-seq). The code for single-cell RNA-seq analyses is accessible at https://github.com/shreyii/scRNA-seqAnalysis.git.

Mouse Studies

All mouse studies complied with the National Research Council Guide for the Care and Use of Laboratory Animals (2011 revision) and conformed to the ARRIVE 2.0 (Animal Research: Reporting of In Vivo Experiments) reporting guidelines. Studies were performed under institutional animal care and use committee protocol 10231 at the University of Alabama at Birmingham and protocols 24-0323 and 21-0359 at Washington University. Male mice, 10 to 12 weeks of age, were studied to reduce experimental variability and overall sample size, given known substantial differences in survival, LV remodeling, and inflammatory responses between male and female mice.[17,18] A total of 475 mice were used.

Human Studies

Peripheral blood was collected from human participants upon initial presentation to the University of Alabama at Birmingham Hospital with acute ST-segment–elevation MI under the auspices of a University of Alabama at Birmingham institutional review board–approved protocol (X151201004). Blood was also collected from control participants (with coronary artery disease but without acute coronary syndrome) before elective percutaneous coronary intervention (PCI) under the auspices of the University of Alabama at Birmingham institutional review board protocol X130807012. Informed consent was obtained from all patients.

Statistical Analysis

All results are presented as mean±SD. Analyses were performed using GraphPad Prism version 7.03 software. Group variances were compared using the Brown-Forsythe test, and normality was assessed using the D'Agostino-Pearson test. Two-group statistical comparisons were performed using an unpaired *t* test with equal or unequal variance (Welch *t* test) for normally distributed variables or Mann-Whitney *U* test for non-normal distribution. For comparisons of >2 groups, experimental data sets were first assessed for normality. For normally distributed data, a 1-way ANOVA was performed, with Bonferroni, Tukey, or Dunnett T3 post-test to adjust for multiple comparisons. For multiple comparisons of groups with unequal variance, Welch ANOVA was used with Dunnett T3 post-test. If a non-normal distribution was observed, the Kruskal-Wallis test was used. Specific approaches are presented in the figure legends. $P<0.05$ was considered significant.

RESULTS

Spleen-Derived, Macrophage-Like CD169+Tim4+ Cells Circulate Within the Ly6Clow Monocyte Compartment and Populate the Heart

Spleens were harvested from naive wild-type (WT) C57BL/6 mice. Immunostaining identified splenic CD169^{+}Tim4^{+} macrophages mainly confined to the MZ (Figure 1A). Using the gating strategy shown in Figure S2A, splenic MMMs (CD45^{+}Ly6C^{-}

CD11b^{low}F4/80^{low}CD169^{+}) were identified by flow cytometry; ≈55% of CD169^{+} MMMs were Tim4^{+} (Figure 1A). Next, using the fluorescence-activated cell sorting (FACS) strategy in Figure S2B, we identified Ly6G^{-}Ly6C^{+}CD169^{+} Tim4^{+} cells in the blood, which were primarily (>95%) in the Ly6C^{low} monocyte compartment (Figure S2B and S2C). May-Grünwald Giemsa staining of FACS-sorted cells revealed a distinct morphology (cell projections) and smaller size than circulating Ly6C^{hi} monocytes (Figure S2D). Further analysis of Ly6C^{low} monocytes revealed a minor subpopulation expressing CD169 (Figure 1B). CD169^{+}Tim4^{+} cells comprised ≈20% of the blood Ly6C^{low} monocytes, and ≈90% of these cells expressed CD64, considered a core macrophage marker,[19–21] and MHC II (major histocompatibility complex class II; Figure 1B), suggesting macrophage-like features. Four weeks after splenectomy, mice exhibited profound (≈70%) reductions in circulating Ly6C^{low}CD169^{+}Tim4^{+} monocytes. splenectomized mice also exhibited mild leukocytosis, neutrophilia, anemia, and thrombocytosis (Figure S3A), but had no changes in circulating B cells, CD4^{+} and CD8^{+} T cells, or Ly6C^{hi} monocytes, and had comparable cardiac size and function (Figure S3B and S3C).

To further explore the identity of blood CD169^{+}Tim4^{+} monocytes, we performed lineage tracing in *Cx3cr1*^{CreERT2};*Rosa26*^{tdTomato} mice in which a tamoxifen pulse labels all Cx3cr1-expressing cells (ie, monocytes,

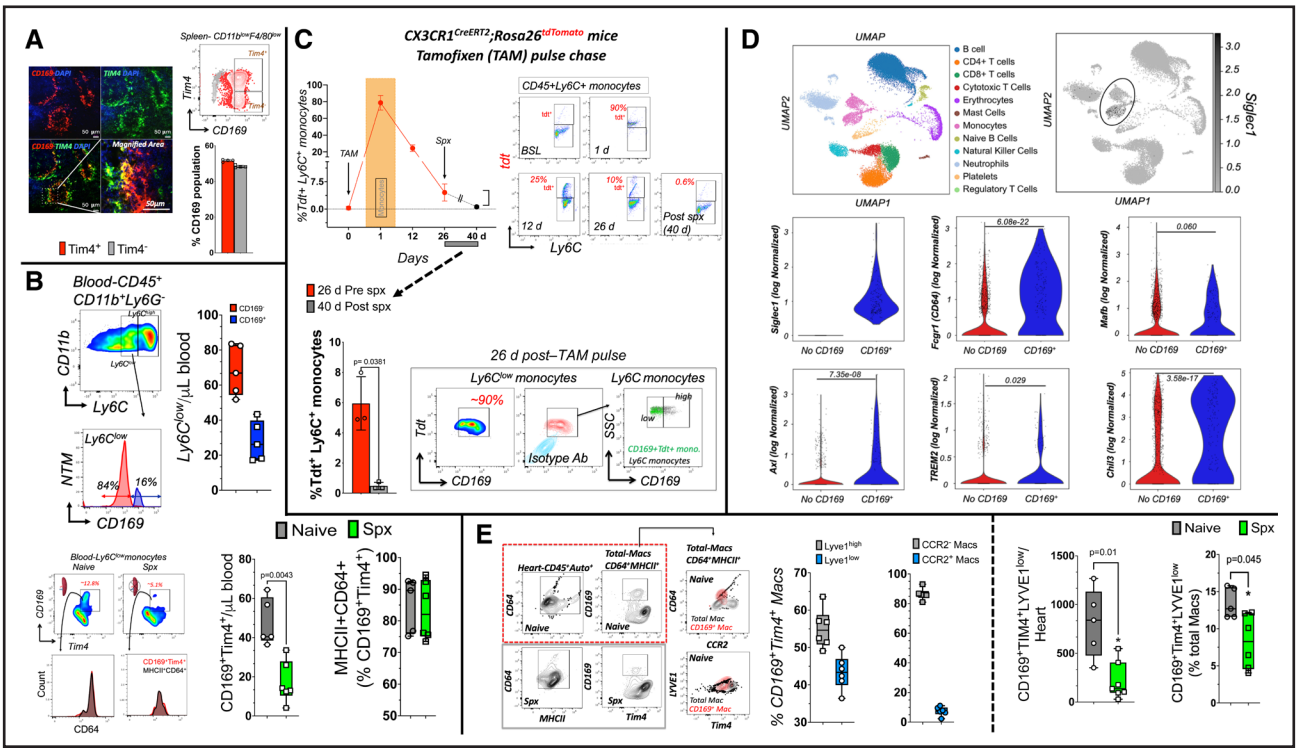

Figure 1. Splenic CD169+Tim4+ marginal metallophilic macrophages circulate as Ly6Clow monocytes and populate the naive heart.

A, **Left**, Representative immunostaining of macrophages in the splenic marginal zone expressing cluster of differentiation (CD) 169 (red) and T cell immunoglobulin– and mucin-domain–containing molecule 4 (Tim4; green), and DAPI nuclear staining (blue). **Right**, Fluorescence-activated cell sorting (FACS) contour plots for CD169 and Tim4 expression in splenic CD45^{+}CD11b^{low}F4/80^{low} cells and quantitation of Tim4 expression in CD169^{+} marginal metallophilic macrophages (n=4). **B**, **Top**, FACS plots of circulating Ly6C (lymphocyte antigen 6 complex, locus C) monocytes with histograms identifying CD169^{+} and CD169^{-} populations within Ly6C^{low} monocytes, and corresponding cell quantitation. **Bottom**, FACS pseudocolor plots of circulating Ly6C^{low}CD169^{+}Tim4^{+} macrophages in naive and splenectomized mice with flow histograms identifying CD64 and MHC II (major histocompatibility complex class II) surface expression (in black), together with quantitation of the populations shown (n=5–7). Mann-Whitney *U* test. **C**, **Top** and **Bottom Left**, Representative blood FACS dot plots and quantitation of tdTomato (Tdt) expression in blood Ly6C^{+} monocytes from CX3CR1^{CreERT2} (C-X3-C motif chemokine receptor 1); Rosa26^{tdTomato} mice after a tamoxifen (TAM) pulse to induce Cre recombination. Also shown are data 14 days after splenectomy performed at 26 days after TAM and quantitation of Tdt^{+}Ly6C^{+} monocytes before and after splenectomy (n=3). *P<0.05; paired *t* test. **Bottom Right**, FACS plots showing CD169 expression in Tdt+ cells 26 days after TAM pulse and overlay of the CD169^{+}Tdt^{+} cells (green) on blood Ly6C^{+} monocytes. **D**, **Top**, Uniform manifold approximation and projection (UMAP) plots from single-cell RNA sequencing of blood leukocytes from 3 naive mice (≈400 000 total cells) identifying 12 cell clusters (**left**) with depiction of CD169 (*Siglec1*) expression levels, primarily observed in the monocyte cluster (**right**). **Middle** and **Bottom**, Violin plots quantitating expression of select macrophage genes in monocytes with and without CD169 expression. Wilcoxon rank-sum test; *P* values are shown in the panel. **E**, **Left**, FACS plots identifying CD169^{+}Tim4^{+} cardiac macrophages in intact and splenectomized mice, overlay of these macrophages on contour plots of CCR2 (C-C motif chemokine receptor 2) and LYVE1 expression (in intact mice), and quantitation of overall LYVE1 and CCR2 expression (n=6). **Right**, Quantitation of frequency and number of cardiac CD169^{+}Tim4^{+}LYVE1^{low} macrophages in naive and splenectomized C57BL/6 mice (n=5–7/group). Unpaired *t* test. NTM indicates normalized to mode.

macrophages, dendritic cells [DCs]) with tdTomato. Given their shorter lifespan, monocytes and DCs generally no longer express tdTomato by 3 weeks as new cells replace them, whereas macrophage (and long-lived monocyte) tdTomato is retained.[22] As illustrated in Figure 1C, 1 day after tamoxifen, ≈80% of Ly6C$^+$ monocytes expressed tdTomato. At 26 days after tamoxifen, ≈6% of total Ly6C$^+$ blood cells remained td-Tomato$^+$, supporting either a long-lived monocyte or macrophage population. Most of these td-Tomato$^+$ cells expressed CD169 and were Ly6C^{low}. Repeat analysis 2 weeks after splenectomy in these mice revealed near total disappearance of circulating Ly6C$^+$tdT$^+$ cells, consistent with a splenic origin for circulating Ly6C^{low}CD169$^+$ monocytes/macrophages.

Single-cell RNA-seq of blood leukocytes from naive mice (Figure 1D) revealed CD169 (*Siglec1*) expression in a minority (14%) of cells identified as monocytes. Compared with monocytes without detectable levels of *Siglec1* transcript, *Siglec1*-expressing cells exhibited significantly higher transcript levels of key macrophage genes *Fcgr1* (*CD64*), *Axl*, *Trem2*, and *Chil3*, and a near significant increase [*P*=0.06] in *Mafb*. Heatmaps for the top 20 upregulated and downregulated differentially expressed genes (DEGs), and key macrophage and DC genes, in *Siglec1*-expressing (versus nonexpressing) cells are shown in Figure S4, together with quantitation of DC genes *Zbtb46*, *Dpp4*, and *Flt3*. Expression levels of DC genes were very low in both CD169$^+$ and CD169$^-$ monocytes. Hence, these results indicate that blood CD169$^+$ cells are unlikely to represent DCs and rather are spleen-derived monocytes with macrophage-like characteristics.

We next characterized cardiac CD169$^+$Tim4$^+$ macrophages and the impact of the spleen. Live/dead staining with 7-aminoactinomycin D (7-AAD) routinely yielded >90% to 95% viability of isolated heart mononuclear cells (Figure S5A). We identified CD64$^+$MHC II$^+$CD169$^+$Tim4$^+$ macrophages using gating strategy 1 in Figure S5B, and used LYVE1, a marker specific for resident macrophages,[14,23,24] to delineate LYVE1^{hi} (cardiac resident[14]) and LYVE1^{low} macrophage subsets. As shown in Figure 1E, cardiac CD169$^+$Tim4$^+$ macrophages were principally (≈90%) CCR2$^-$ (C-C motif chemokine receptor 2) but exhibited variable LYVE1 expression, with ≈40% to 45% being LYVE1^{low}. Splenectomized mice exhibited significant reduction (≈80%) of cardiac CD169$^+$Tim4$^+$LYVE1^{low} macrophages (Figure 1E) without significant change in the LYVE1^{hi} subset (Figure S6A). Principal component analysis of bulk RNA-seq of sorted CD64$^+$MHC II$^+$CD169$^+$Tim4$^+$ cardiac macrophages revealed separation based on LYVE1 expression, with 987 DEGs (q<0.05) and discrete clustering of LYVE1^{hi} and LYVE1^{low} cells, suggesting distinct functional subsets (Figure S6B). Moreover, expression analysis of 54 select macrophage- and DC-associated genes[25–27] revealed that both subsets expressed macrophage marker genes, but uniformly low levels of DC-associated genes (Figure S6C). Intravascular CD45 labeling in vivo immediately before cardiac harvest in a subset of mice (Figure S7) revealed that intravascular leukocytes comprised ≈0.5% of cardiac CD169$^+$Tim4$^+$ cells isolated at steady state, and <2% 24 hours after MI, confirming tissue localization. These findings collectively are consistent with splenic CD169$^+$Tim4$^+$ macrophages circulating as Ly6C^{low}CD64$^+$CD169$^+$Tim4$^+$ macrophage-like monocytes that help populate CD169$^+$Tim4$^+$CCR2$^-$LYVE1^{low} macrophages in the heart.

Splenic CD169+Tim4+ Macrophages Augment Cardiac Trafficking and Phagocytosis Acutely After MI

WT mice were evaluated 24 hours after nonreperfused MI, during the inflammatory phase of repair. Compared with sham-operated mice, there was a ≈3-fold increase in blood CD169$^+$Tim4$^+$ monocytes 24 hours after MI (Figure 2A). CCR3 and CCR4 expression increased in circulating CD169$^+$Tim4$^+$ monocytes (Figure 2B) along with upregulation of cognate chemokine ligands in border zone myocardium, including C-C chemokine ligand (CCL) 5, CCL6, CCL7, CCL17, and CCL22.[28] In contrast, splenectomized mice did not exhibit increases in circulating CD169$^+$Tim4$^+$ cells 24 hours after MI (Figure 2C). We next examined CD169$^+$Tim4$^+$ macrophage infiltration in the acutely infarcted heart. Here, to align with previous studies of MMMs in the spleen, and to maintain consistency between approaches in blood and heart given dynamic innate immune cell flux acutely after MI, we used low expression of Ly6C as a central identifier of CD169$^+$Tim4$^+$ macrophages, as illustrated in Figure S5B, gating strategy 2. As shown in Figure 2D, WT mice exhibited a robust ≈2.5-fold increase in cardiac CD169$^+$Tim4$^+$ macrophages 1 day after MI. Overall cell numbers were reduced in splenectomized mice and the increase after MI was abrogated. Concomitantly, the spleen in MI mice exhibited dynamic changes with significant hypotrophy and loss of marginal metallophilic macrophages, consistent with egress from the spleen (Figure 2E). We next evaluated phagocytic activity of Ly6C^{low}CD169$^+$Tim4$^+$ macrophages. Fluorescent bioparticles were given intravenously 3 hours before sacrifice with determination of cell bioparticle uptake by FACS. As shown in Figure 2F, there was a significant (≈2-fold) increased uptake of bioparticles by CD169$^+$Tim4$^+$ cells in both blood and heart versus sham mice, establishing enhanced phagocytic capacity of these macrophages after MI. There was an attendant reduction of CD169$^+$Tim4$^+$bioparticle$^+$ macrophages in the spleen, consistent with overall fewer MMMs early after MI.

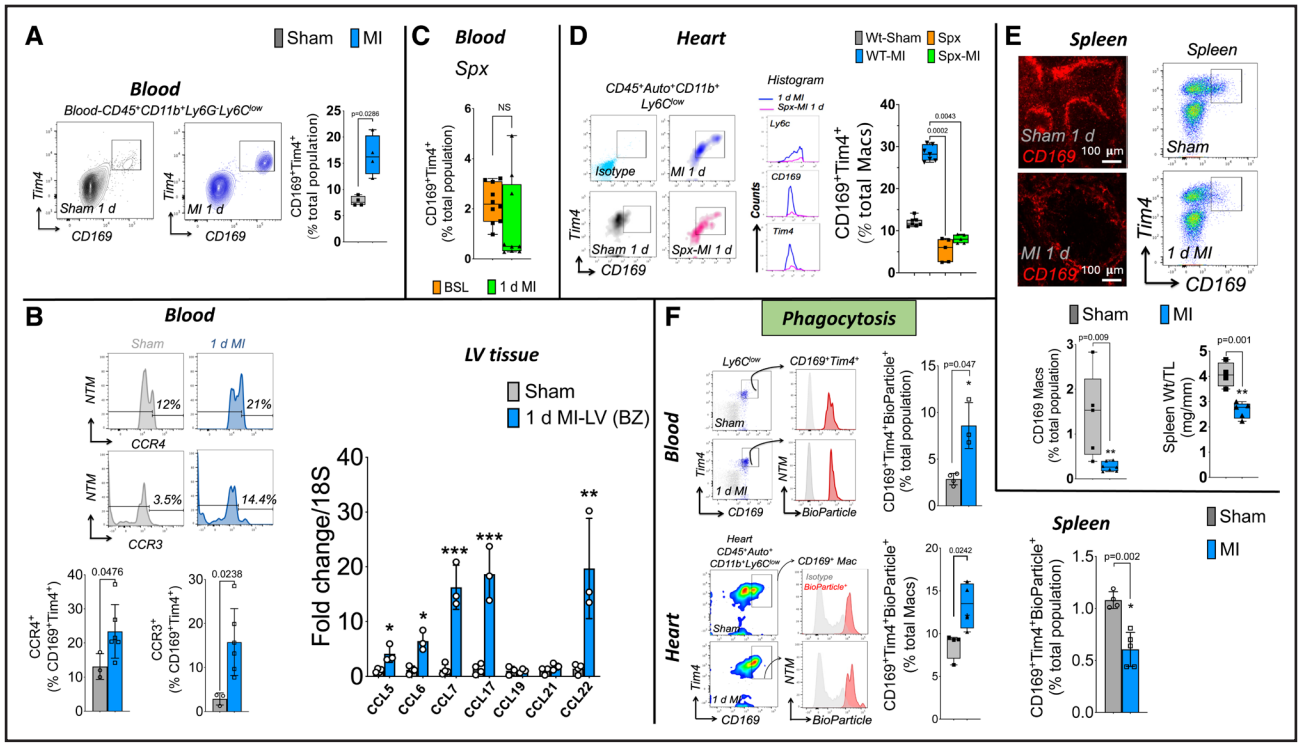

Figure 2. Splenic marginal metallophilic macrophages increase cardiac trafficking and exhibit phagocytosis after acute myocardial infarction.

A, Fluorescence-activated cell sorting (FACS) plots and group quantitation for circulating Ly6C^{low}CD169^{+}Tim4^{+} (lymphocyte antigen 6 complex, locus C; cluster of differentiation 169; T cell immunoglobulin– and mucin-domain–containing molecule 4) monocytes in wild-type (WT) C57BL/6 mice 1 day after myocardial infarction (MI) or sham operation (n=4/group). Mann-Whitney *U* test. **B**, **Left**, Flow histograms demonstrating surface expression of CCR (C-C motif chemokine receptor) 3 and CCR4 in Ly6C^{low}CD169^{+}Tim4^{+} monocytes from the same groups. Unpaired *t* test; *y* axis represents cell counts. **Right**, Chemokine gene expression by reverse transcription polymerase chain reaction (normalized to 18 seconds) in the myocardial border zone (BZ) 1 day after MI or sham operation (n=4 or 5/group). Unpaired *t* test. **P*<0.05, ***P*<0.01, ****P*<0.001 vs sham. **C**, Circulating Ly6C^{low}CD169^{+}Tim4^{+} cell frequency before and 1 day after MI in splenectomized mice (n=9). Mann-Whitney *U* test. **D**, FACS density plots, histograms, and quantitation of cardiac Ly6C^{low}CD169^{+}Tim4^{+} macrophages in WT and splenectomized mice 1 day after MI or sham operation (n=4–7/group). Kruskal-Wallis test. **E**, Immunostains and FACS dot plots of splenic CD169^{+} metallophilic marginal macrophages (red) 24 hours after MI or sham operation, and quantitation of metallophilic marginal macrophage frequency by FACS and spleen weight (n=5–7/group). Unpaired *t* test. **F**, **Left**, FACS dot plots and histograms, and corresponding quantitation, of blood and heart Ly6C^{low}CD169^{+}Tim4^{+}Bioparticle^{+} cells from sham and MI mice given 10 mg/kg Texas Red–conjugated bioparticles IV 3 hours before sacrifice (n=3 or 4/group). Unpaired *t* test for blood and nonparametric Mann-Whitney *U* test for heart (non-normal distribution). **Right**, Quantitation of splenic BioParticle^{+} metallophilic marginal macrophages in the same experimental mouse groups. Unpaired *t* test. BSL indicates baseline; NS, not significant; NTM, normalized to mode; and TL, tibia length.

To definitively establish a splenic source for CD169^{+}Tim4^{+} macrophages in the acutely infarcted heart, we used parabiosis. The circulations of CD45 isotype-mismatched mice were surgically joined, with nonreperfused MI induced 4 weeks later in either intact or splenectomized host mice (Figure S8). Blood FACS (2 days after MI) indicated stable ≈35% donor chimerism of CD45^{+} blood leukocytes in both intact and splenectomized host mice (Figure S8; Figure 3A). We then evaluated cardiac CD169^{+} macrophages using gating strategy 2 in Figure S5B. In hearts of intact host MI mice, ≈15% of CD169^{+} macrophages were of donor origin; donor chimerism significantly increased by 138% in splenectomized host MI mice (Figure 3A), consistent with augmented sourcing from the parabiont donor spleen.

For more comprehensive validation, we examined host CD169^{DTR} mice expressing human diphtheria toxin (DT) receptor (DTR) in the sialoadhesin gene, allowing selective depletion of CD169^{+} macrophages,[11] and parabiont macrophage Fas-induced apoptosis (MaFIA) mice expressing GFP (green fluorescent protein) in all mononuclear phagocytes, and used gating strategy 1 in Figure S5B to identify cardiac CD169^{+}Tim4^{+} macrophages. In the first set of experiments, host CD169^{DTR} mice received either vehicle or DT (10 µg/kg IP) at the time of MI, and host cardiac leukocytes were examined 2 days later. As shown in Figure 3B, compared with vehicle, DT-treated host mice exhibited robust increases in the frequency of parabiont-derived cardiac GFP^{+} leukocytes and GFP^{+}CD169^{+}Tim4^{+} macrophages, despite a reduction in total CD169^{+}Tim4^{+} cells (expressed as percent of total cardiac macrophages). These data establish increased sourcing of cardiac CD169^{+} macrophages from the parabiont circulation after CD169^{+} cell ablation

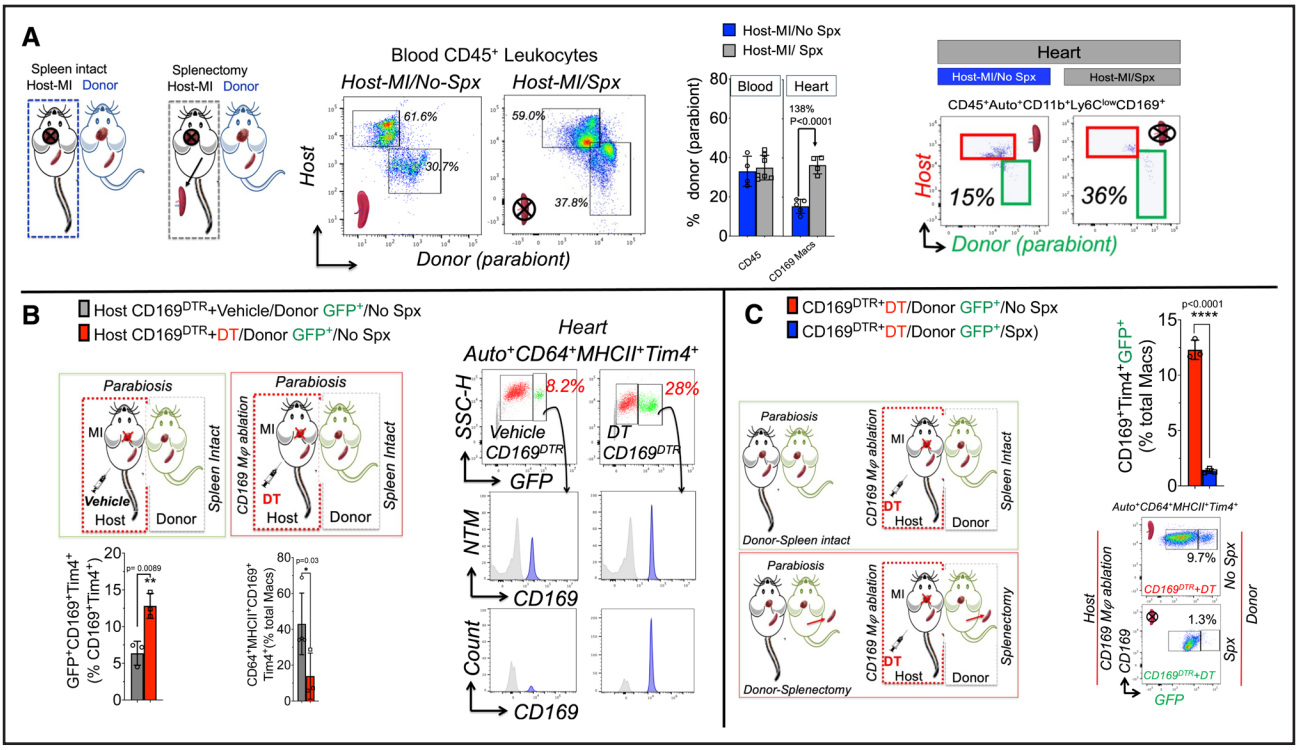

Figure 3. CD169+Tim4+ macrophages in the acutely infarcted heart depend on the spleen.
A, **Left**, Parabiosis schema joining cluster of differentiation (CD) 45 isotype–mismatched host (spleen-intact or after splenectomy) and donor parabiont mice, with myocardial infarction (MI) induced in the host. **Middle** and **Right**, Fluorescence-activated cell sorting plots and quantitation of donor chimerism in host mouse blood (total CD45+ leukocytes) and heart (Ly6C^{low}CD169+ [lymphocyte antigen 6 complex, locus C; cluster of differentiation 169] macrophages) in spleen-intact and splenectomized host mice 48 hours after MI (n=4–7/group). **B**, **Top Left**, Parabiosis schema joining CD169^{DTR} host and donor parabiont macrophage Fas-induced apoptosis (MaFIA) mice, with host mice given either vehicle or diphtheria toxin (DT) at the time of MI. **Right**, Representative fluorescence-activated cell sorting dot plots of donor GFP+CD169+ (green fluorescent protein; CD169) macrophages in 48 hours post-MI hearts from host mice and flow histograms of CD169 expression in GFP+CD64+MHC II+Tim4+ cells delineated as normalized to mode (NTM) or cell counts. **Bottom Left**, Quantitation of GFP+ frequency in host cardiac CD169+Tim4+ macrophages and total CD169+Tim4+ cells as a percentage of all autofluorescent (Auto)+ macrophages in vehicle and DT-treated host MI mice (n=3 or 4/group). **C**, **Left**, Parabiosis schema joining CD169^{DTR} host mice and either spleen-intact or splenectomized MaFIA donor parabionts, with host mice given DT at the time of MI to deplete CD169+ macrophages. **Right**, Example fluorescence-activated cell sorting dot plots and quantitation of donor CD45+Auto+CD64+MHC II+GFP+CD169+Tim4+ macrophages in the host MI heart 48 hours after MI (n=3 or 4/group). Welch *t* test. MHC II indicates major histocompatibility complex class II.

in the host. In the second set of studies, host CD169^{DTR} mice receiving DT at the time of MI were paired with either intact or splenectomized MaFIA parabionts, and host GFP+CD169+ cardiac macrophages were measured after 2 days. Compared with CD169^{DTR} mice paired with intact MaFIA parabionts, the hearts of host CD169^{DTR} mice paired with splenectomized MaFIA mice exhibited profoundly reduced GFP+CD169+ macrophages (Figure 3C). These data establish splenic dependence of augmented cardiac CD169+ macrophages from the parabiont circulation upon host CD169+ cell ablation.

We next evaluated the impact of MI, and the spleen, on cardiac CD169+Tim4+ macrophage LYVE1 subsets, using gating strategy 1 in Figure S5B. In naive hearts, LYVE1^{hi} resident cells comprised the majority of CD169+Tim4+ macrophages (≈60%) versus LYVE1^{low} (Figures 4A and 1E). One day after MI, this ratio reversed, with a marked decrease (≈1.8-fold) in LYVE1^{hi} frequency (consistent with ischemic loss[14,24]) and ≈3.5-fold increase in LYVE1^{low} macrophages (Figure 4A). Bulk RNA-seq of sorted LYVE1^{hi} and LYVE1^{low} cardiac CD169+Tim4+ macrophages 1 day after MI revealed 462 DEGs ($q<0.05$) and subset segregation by hierarchical clustering (Figure 4B). Gene Ontology pathway analysis revealed higher expression of metabolism and oxidative phosphorylation genes and lower expression of immune response genes in the LYVE1^{low} subpopulation in the acutely infarcted heart (Figure S9A), suggesting an immunomodulatory and proresolving phenotype. Moreover, gene expression analysis of the LYVE1^{low} subset (versus LYVE1^{hi} cells) revealed upregulation of several genes related to tissue injury (*Egr1*), wound healing, cell migration, matrix responses (*Thbs1*, *Nrp1*, *Mmp9*, and *Mmp12*), and immunomodulation (*Socs3* and *Sem4a*), consistent with a reparative and healing role for CD169+Tim4+LYVE1^{low} macrophages (Figure S9B). These differences were much more pronounced after

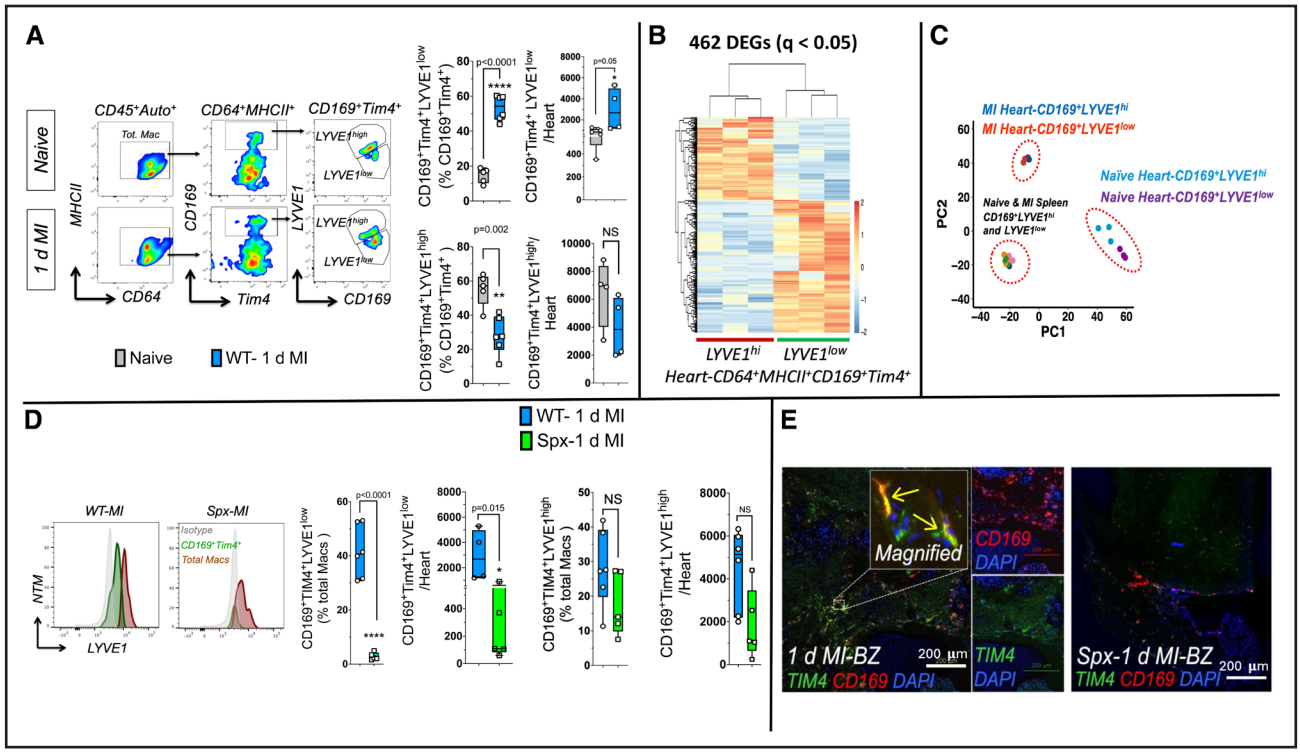

Figure 4. Spleen-dependent CD169+Tim4+LYVE1low macrophages expand in the acutely infarcted heart.
A, **Left**, Fluorescence-activated cell sorting pseudocolor plots of cardiac CD169^{+}Tim4^{+} (cluster of differentiation 169; T cell immunoglobulin– and mucin-domain–containing molecule 4) macrophages and separation based on LYVE1 (lymphatic vessel endothelial hyaluronan receptor 1) surface expression in naive and 1 day after myocardial infarction (MI) mice. **Right**, Quantitation of LYVE1^{hi} and LYVE1^{low} CD169^{+}Tim4^{+} macrophages in hearts from naive and 1 day after MI mice (n=4–6/group). Unpaired *t* test. **B**, Heatmap of 462 significant ($P_{adjusted}$<0.05) differentially expressed genes (DEGs) by RNA sequencing analysis in sorted LYVE1^{hi} and LYVE1^{low} CD169^{+}Tim4^{+} cardiac macrophages 1 day after MI. **C**, Principal component analysis plots using the top 500 DEGs after rlog transformation of RNA sequencing data from macrophages sorted from the indicated sites in naive and 1 day after MI mice. **D**, **Left**, Flow histograms depicting LYVE1 surface expression on cardiac CD169^{+}Tim4^{+} macrophages (green) and total autofluorescence^{+}CD64^{+}MHC II^{+} macrophages (brown) in wild-type (WT) and splenectomized mice 1 day after MI. **Right**, Fluorescence-activated cell sorting quantitation of LYVE1^{hi} and LYVE1^{low} CD169^{+}Tim4^{+} macrophages in the hearts of WT and splenectomized mice 1 day after MI (n=5 or 6/group). Unpaired *t* test. **E**, Representative confocal micrograph of border zone (BZ) myocardium immunostained for CD169 (red) and Tim4 (green) 1 day after MI in WT and splenectomized mice, and nuclear staining with DAPI (blue). Scale bar=200 µm. Inset shows magnified images of CD169 and Tim4 staining. Yellow arrows indicate double-positive cells. Scale bar=10 µm. MHC II indicates major histocompatibility complex class II. NTM indicates normalized to mode.

MI compared with naive conditions. Principal component analysis of RNA-seq data from LYVE1^{hi} and LYVE1^{low} CD169^{+} cardiac and splenic macrophages from naive and post-MI mice revealed tight clustering of splenic cells regardless of underlying condition, but distinct clustering of cardiac macrophages linked to underlying injury, suggesting an overriding influence of tissue microenvironment on CD169^{+} macrophage phenotype (Figure 4C). Splenectomized mice failed to expand CD169^{+}Tim4^{+}LYVE1^{low} cardiac macrophages after acute MI, exhibiting profoundly (≈11-fold) diminished levels of these cells compared with WT MI mice (Figure 4D and 4E). These data collectively establish that splenic CD169^{+}Tim4^{+} MMMs with phagocytic capacity acutely traffic as Ly6C^{low}CD169^{+}Tim4^{+} monocytes to the heart after MI in response to chemotactic signals and are a primary source of immunomodulatory and proresolving CD169^{+}Tim4^{+}LyVE1^{low} macrophages in the infarcted heart.

CD169+ Macrophages and the Spleen Promote Apoptotic Neutrophil Clearance, Suppress Neutrophil Activation, and Resolve Inflammation After MI

Coronary ligation was performed in WT mice, splenectomized mice, and CD169^{DTR} mice (given DT 1 hour after ligation), with evaluation 24 hours later. Relative to WT mice, both splenectomized mice and CD169^{DTR}/DT mice exhibited marked reductions in blood Ly6C^{low}CD169^{+}Tim4^{+} and total Ly6C^{low} monocytes after acute MI (Figure 5A), without changes in Ly6C^{hi} monocytes (Figure S10A). Levels of Ly6C^{low}CD169^{+}Tim4^{+} macrophages and total Ly6C^{low} cells in the heart 24 hours after MI were profoundly reduced in both splenectomized mice and CD169^{DTR}/DT mice (Figure 5B), again without differences in Ly6C^{hi} cells (Figure S10B). In contrast, compared with WT, both splenectomized mice and CD169^{DTR}/DT mice exhibited significantly elevated

levels of blood neutrophils (and activated ICAM$^+$ neutrophils) 24 hours after MI (Figure 5C), indicative of heightened acute inflammation.

Macrophage ingestion of apoptotic cells suppresses the production of proinflammatory mediators and promotes secretion of proresolving cytokines, including interleukin (IL)−10 and transforming growth factor β.[29,30] During acute MI, apoptotic neutrophils undergo efferocytosis by macrophages.[1,6] As shown in Figure 5D and Figure S10C, compared with WT, both splenectomized and CD169^{DTR}/DT mice exhibited augmented cardiac neutrophil infiltration and increased annexin V$^+$ apoptotic neutrophils after acute MI, as assessed by immunostaining and FACS. Neutrophilia in splenectomized and CD169^{DTR}/DT mice was accompanied by increased Lin$^-$cKit$^+$CD34$^+$CD16/32$^+$ granulocyte-macrophage progenitors in the bone marrow, suggesting augmented granulopoiesis upon loss of splenic MMMs (Figure 5E). To establish a role for CD169$^+$Tim4$^+$ macrophages in neutrophil efferocytosis, experiments were performed in Catchup mice,[31] which contain a knock-in allele expressing Cre recombinase and the fluorescent protein tdTomato in the first exon of Ly6G. As depicted in Figure 5F, tdTomato-positive neutrophils were identified in the heart 24 hours after MI in these mice; ≈50% of CD169$^+$Tim4$^+$ macrophages in the acutely infarcted heart also exhibited tdTomato fluorescence, indicating the presence of ingested apoptotic neutrophils.

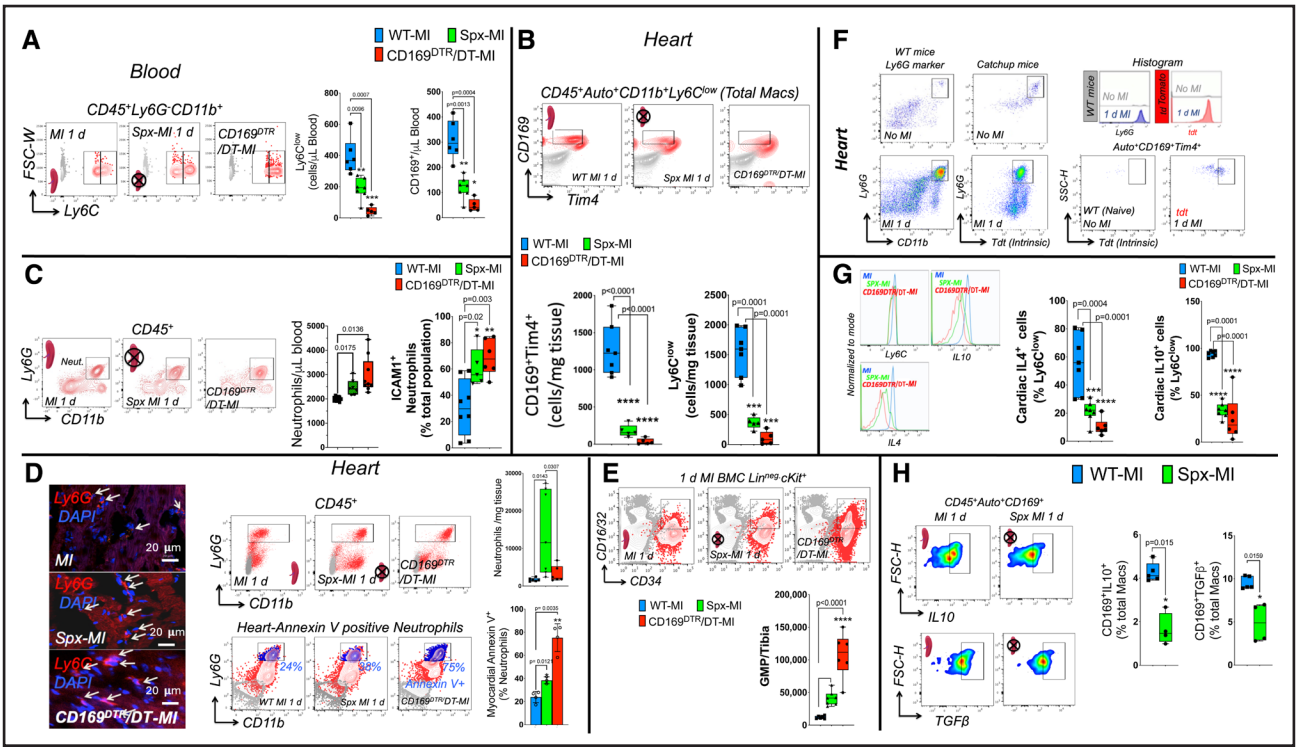

Figure 5. CD169+Tim4+ macrophages clear apoptotic neutrophils, suppress neutrophil activation, and resolve inflammation after myocardial infarction.

Fluorescence-activated cell sorting (FACS) plots and quantitation of Ly6C^{low}CD169$^+$Tim4$^+$ (lymphocyte antigen 6 complex, locus C; cluster of differentiation 169; T cell immunoglobulin– and mucin-domain–containing molecule 4) monocytes/macrophages and total Ly6C^{low} cells in blood (**A**) and in heart (**B**) 1 day after myocardial infarction (MI) in wild-type (WT) and splenectomized WT mice, and CD169^{DTR} mice given diphtheria toxin (CD169^{DTR}/DT) at the time of MI (n=5–7/group). **A**, Welch ANOVA, Dunnett T3 post-test; **B**, 1-way ANOVA, Bonferroni post-test. Isotype antibody is shown in gray. **C**, FACS plots and group data for blood CD45$^+$CD11b$^+$Ly6G$^+$ neutrophils and ICAM-1/CD54$^+$ neutrophils 1 day after MI in WT, splenectomized, and CD169^{DTR}/DT mice (n=6–8/group). One-way ANOVA, Bonferroni post-test. **D**, **Left**, Representative confocal images of immunofluorescent Ly6G staining in WT, splenectomized, and CD169^{DTR}/DT hearts 1 day after MI demonstrating Ly6G$^+$ neutrophil (red) infiltration (arrows), and nuclear staining with DAPI (blue). Scale bar=20 µm. Right, FACS plots and corresponding quantitation of cardiac CD45$^+$CD11b$^+$Ly6G$^+$ neutrophils (red) and annexin V$^+$ apoptotic neutrophils (blue) in the same groups 1 day after MI (n=3 or 4/group). One-way ANOVA, Dunnett T3 post-test. **E**, FACS density plots for Lin$^-$c-kit$^+$CD34$^+$CD16/32$^+$ granulocyte monocyte precursors (GMPs) in bone marrow from WT, splenectomized, and CD169^{DTR}/DT mice 1 day after MI, together with quantitation. Flow gates were based on isotype antibody control (n=5–7/group). One-way ANOVA, Tukey post-test. **F**, **Left**, Representative FACS dot plots identifying cardiac neutrophils as CD11b$^+$Ly6G$^+$ cells in WT mice and as Ly6G$^+$tdTomato$^+$ cells in Catchup mice at baseline and 1 day after MI. **Top Right**, Representative histograms of Ly6G and tdTomato fluorescence intensity in heart mononuclear cells from the same groups. **Bottom Right**, FACS dot plots gated on cardiac CD169$^+$Tim4$^+$ macrophages illustrating tdTomato expression in Catchup mice 1 day after MI. **G**, Representative FACS histograms of intracellular interleukin (IL)−4 and IL-10 staining in cardiac Ly6C^{low} cells 1 day after MI in WT, splenectomized, and CD169^{DTR}/DT mice, together with cell quantitation of the Ly6C^{low} subsets (n=6 or 7/group). One-way ANOVA, Bonferroni post-test. **H**, Representative FACS pseudocolor plots for intracellular TGFβ (transforming growth factor-β) and IL-10 staining in cardiac CD169$^+$ macrophages 1 day after MI in WT and splenectomized mice, with accompanying quantitation (n=4 or 5/group). Unpaired *t* test. BMC indicates bone marrow cells.

Reduced neutrophil efferocytosis in the absence of splenic CD169^{+}Tim4^{+} macrophages after MI would delay tissue macrophage polarization toward a reparative phenotype. Indeed, flow cytometric evaluation of cardiac Ly6C^{low} cells 24 hours after MI indicated profoundly reduced anti-inflammatory IL-10 and IL-4 expression in splenectomized and CD169^{DTR}/DT mice compared with WT mice (Figure 5G). CD169^{+} macrophages in the acutely infarcted heart exhibited ≈2-fold lower IL-10^{+} and transforming growth factor β^{+} cells in splenectomized MI mice compared with WT MI mice (Figure 5H), and F4/80 and IL-10 immunostaining of the infarct border zone revealed significantly fewer dual F4/80^{+}IL-10^{+} (yellow) cells in splenectomized MI mice (Figure S10D). Taken together, these results demonstrate that CD169^{+}Tim4^{+} macrophages, including those of splenic origin, temper the neutrophil inflammatory response and promote efferocytosis and the transition to a proresolving milieu in the heart after acute MI.

Splenic CD169+Tim4+ Macrophages Promote Post-MI Healing and Reduce Adverse LV Remodeling

WT mice, splenectomized mice, and CD169^{DTR}/DT mice underwent nonreperfused MI or sham operation and were followed for 10 days. Compared with respective sham mice, all MI mice exhibited increased mortality over 10 days (Figure 6A). However, post-MI mortality was dramatically, and comparably, higher in both splenectomized mice and CD169^{DTR}/DT mice versus WT mice. Necropsy revealed increased mortality attributable to more frequent cardiac rupture (Figure 6B), consistent with impaired post-MI wound healing in both splenectomized and CD169^{DTR}/DT mice.

To assess the sufficiency of splenic MMMs for cardiac repair, CD45.2 WT splenectomized mice underwent MI, but with intravenous adoptive transfer 24 hours after MI of 1×10^{6} FACS-sorted CD169^{+}Tim4^{+} cells (≈100 µL/mouse) from the spleens of naive donor CD45.1 WT mice (Figure S11A). After adoptive transfer (24 hours), CD45.1^{+}CD169^{+}Tim4^{+} macrophages/monocytes were readily identified in the heart and blood by immunostaining and flow cytometry (Figure S11B), indicating successful donor cell transfer, with recipient splenectomized MI mice augmenting circulating Ly6c^{low}CD169^{+}Tim4^{+} monocytes to levels comparable with nonsplenectomized MI mice (Figure S11C). Splenic CD169^{+}Tim4^{+} cell reconstitution rescued the increased mortality and rupture rate in splenectomized MI mice (Figure 6A and 6B), reduced bone marrow neutrophil levels (Figure S11D), and markedly diminished the abundance (≈13-fold) of both total and annexin V^{+} neutrophils in the infarcted heart 24 hours after transfer (Figure S11E), indicating that splenic MMMs are both necessary and sufficient for tissue repair, temper acute neutrophil inflammation, and augment apoptotic neutrophil efferocytosis. Loss of these specialized macrophages contributes substantially to deleterious post-MI healing in splenectomized mice.

Echocardiography 10 days after MI revealed significantly larger LV end-diastolic volume (EDV) and end-systolic volume (ESV) and lower LV ejection fraction (EF) in splenectomized and CD169^{DTR}/DT MI mice versus WT MI mice (Figure 6C), indicative of exacerbated LV remodeling. Splenic MMM reconstitution in splenectomized MI mice improved LV remodeling, evidenced by significantly lower EDV and ESV (comparable with WT MI mice) versus splenectomized MI mice (Figure 6C). Reparative CD206^{+} macrophages are an important cardiac macrophage population 10 days after MI.[1,5,32] Although CD206^{+} cells were readily identifiable upon border zone immunostaining in all mouse MI groups (Figure 6D), both splenectomized and CD169^{DTR}/DT MI mice exhibited a ≈2.5-fold increase in CD206^{+} macrophages coexpressing proinflammatory inducible nitric oxide synthase (iNOS). Splenic MMM transfer in splenectomized mice markedly decreased (≈4-fold) iNOS^{+}CD206^{+} cardiac macrophages after MI to levels similar to WT mice. Abundance of cardiac iNOS^{-}CD206^{+} cells was comparable across all MI groups (Figure 6D). Accompanying this persistent proinflammatory milieu, there was significantly less border zone matrix metalloproteinase-9 abundance and fibrosis 10 days after MI in both splenectomized and CD169-ablated MI mice, with restoration of matrix metalloproteinase-9 and border zone fibrosis upon splenic MMM transfer in splenectomized MI mice (Figure 6E). These tissue-level changes were accompanied by parallel directional changes in proinflammatory Ly6C^{hi} monocytes and serum levels of anti-inflammatory IL-10 (Figure 6F). In a subgroup of WT, splenectomized, and CD169^{DTR}/DT mice, long-term (8 weeks) post-MI remodeling was examined (Figure S12). Compared with WT MI mice, splenectomized and CD169^{DTR}/DT MI mice exhibited aggravated LV remodeling and HF, with increased chamber volume, greater heart and lung weight, and lower EF; thinner scars and reduced border zone fibrosis; and chronic inflammation with persistently augmented iNOS^{+}CD206^{+} cardiac macrophages.

These findings collectively indicate that splenic CD169^{+}Tim4^{+} macrophages are indispensable for efferocytosis and inflammation resolution, matrix turnover, wound healing and scar formation, and effective remodeling of the post-MI heart. Deficiency of CD169^{+} macrophages early after MI exacerbates LV rupture, adverse long-term LV remodeling, and late HF.

Splenic MZ Expansion Ameliorates Adverse LV Remodeling and Inflammation After MI

Liver X receptor α (LXRα) is a nuclear receptor essential for generation of splenic MZMs. LXRα enhances macrophage phagocytosis and suppresses inflammatory

ORIGINAL RESEARCH ARTICLE

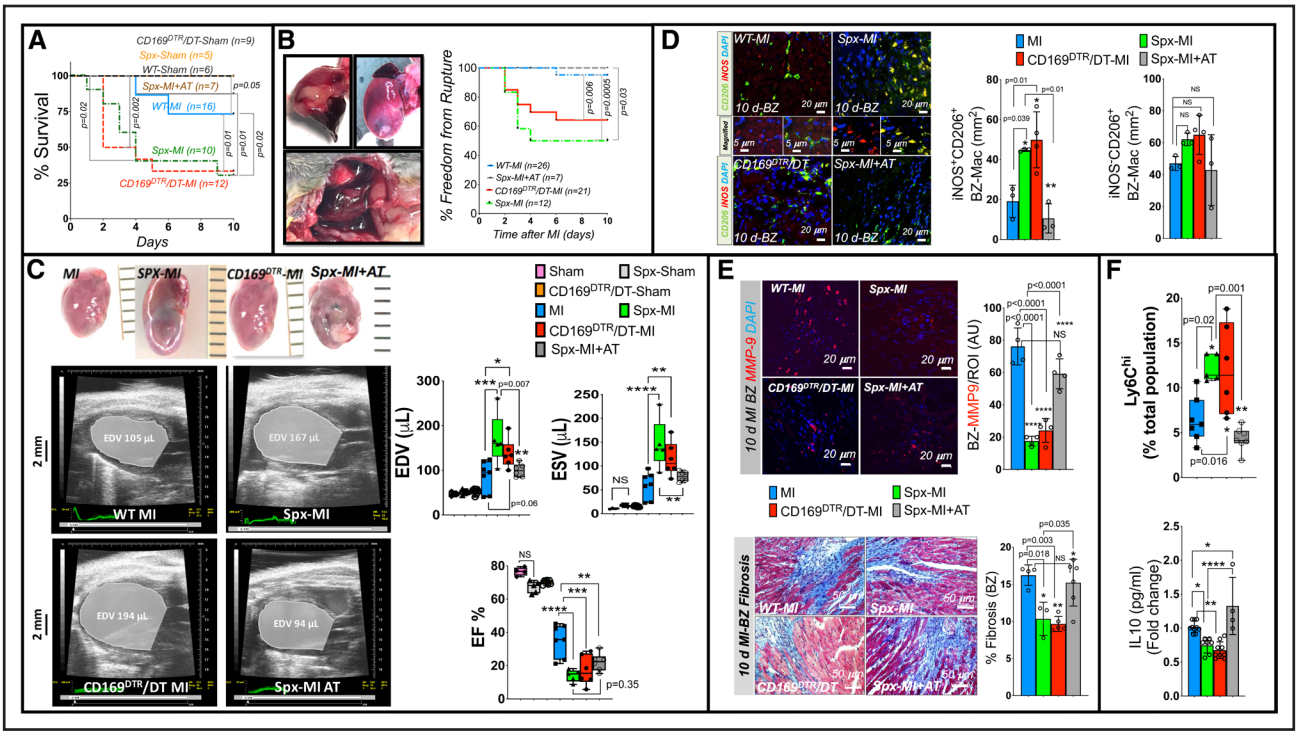

Figure 6. Splenic CD169+Tim4+ marginal metallophilic macrophages promote healing and reduce adverse left ventricular remodeling after myocardial infarction.

A, Ten-day Kaplan-Meier survival curves for cluster of differentiation (CD) 45.2 wild-type (WT), splenectomized, and CD169^{DTR}/diphtheria toxin (DT) mice after myocardial infarction (MI) or sham operation, and for CD45.2 splenectomized MI mice with adoptive transfer of CD45.1 WT naive splenic CD169^{+}Tim4^{+} (CD169; T cell immunoglobulin– and mucin-domain–containing molecule 4) cells 24 hours after MI (splenectomized MI+adoptive transfer [AT]). Log-rank test. **B**, Gross images of post-MI cardiac rupture with hemothorax or hemopericardium, and Kaplan-Meier curves for freedom from rupture over 10 days after MI in WT, splenectomized, CD169^{DTR}/DT, and splenectomized MI+AT mice. Log-rank test. **C**, **Left**, Representative postmortem whole hearts and end-diastolic long-axis 2-dimensional echocardiograms from WT MI, splenectomized MI, CD169^{DTR}/DT MI, and splenectomized MI+AT mice 10 days after MI. Right, Quantitation of left ventricular ejection fraction and end-diastolic volume (EDV) and end-systolic volume (ESV) 10 days after MI or sham for indicated groups (n=4–6/group). One-way ANOVA, Bonferroni post-test. **D**, **Left**, Representative confocal images of immunofluorescent staining for CD206 (green) and inducible nitric oxide synthase (iNOS; red) in the heart infarct border zone (BZ) from WT MI, splenectomized MI, CD169^{DTR}/DT MI, and splenectomized MI+AT mice 10 days after MI. DAPI (blue) nuclear staining. iNOS^{+}CD206^{+} cells appear yellow. Higher magnification is shown in the **middle**. **Right**, Quantitation of iNOS^{+}CD206^{+} and iNOS^{-}CD206^{+} cells/mm^{2} in the hearts (n=3/group). One-way ANOVA, Bonferroni post-test. **E**, **Top Left**, Confocal images of matrix metalloproteinase-9 (MMP-9) immunostaining (red) in infarct BZ of hearts from WT MI, splenectomized MI, CD169^{DTR}/DT MI, and splenectomized MI+AT mice 10 days after MI. Nuclear staining with DAPI (blue). **Top Right**, Quantitative group data for total MMP-9 mean fluorescence intensity per region of interest (ROI; n=4/group). One-way ANOVA, Bonferroni post-test. **Bottom**, Representative Masson trichrome stains of infarcted hearts (10 days after MI) from the same groups demonstrating MI border zone (BZ) fibrosis, together with BZ fibrosis quantitation (n=4/group). One-way ANOVA, Bonferroni post-test. **F**, Fluorescence-activated cell sorting quantitation of Ly6C^{hi} (lymphocyte antigen 6 complex, locus C) blood monocytes and serum interleukin (IL)–10 levels in WT MI, splenectomized MI, CD169^{DTR}/DT MI, and splenectomized MI+AT mice at 10 days after MI (n=4–7/group). One-way ANOVA, Bonferroni post-test. AU indicates arbitrary units; and NS, not significant.

pathways after efferocytosis.[33,34] In naive mice, the selective LXRα agonist T0901317[35] (40 mg/kg IP) induced an ≈9-fold increase in blood CD169^{+}Tim4^{+} monocytes and an ≈1.5-fold expansion of splenic CD169^{+}Tim4^{+} MMMs 24 hours later (Figure S13). To evaluate the effects of splenic MZ expansion during MI, we administered T0901317 40 mg/kg IP daily from 1 day before to 5 days after MI in WT and splenectomized mice (Figure 7A). T0901317 increased CD169^{+}Tim4^{+} macrophages in the heart 24 hours after MI and blood CD169^{+}Tim4^{+} macrophages 10 days after MI in WT MI mice, but not in splenectomized MI mice (Figure 7B). T0901317-treated WT MI mice exhibited significantly improved 10 days post-MI mortality compared with untreated MI mice (Figure 7C), but post-MI mortality was not improved in splenectomized mice. The mortality benefit resulted primarily from reduced ventricular rupture, consistent with improved wound healing.

At 10 days after MI, T0901317-treated WT MI mice exhibited significantly smaller EDV and ESV and higher EF than untreated WT MI mice (Figure 7D). In contrast, there was no effect of T0901317 on LV volumes and EF in splenectomized MI mice. Evaluation of a separate group of WT MI mice 8 weeks after MI revealed that T0901317 given early after MI significantly improved (versus vehicle) long-term survival, LVEDV, LVESV, and LVEF (Figure 7E). There was less total cardiac interstitial fibrosis (border and remote zone) and fewer

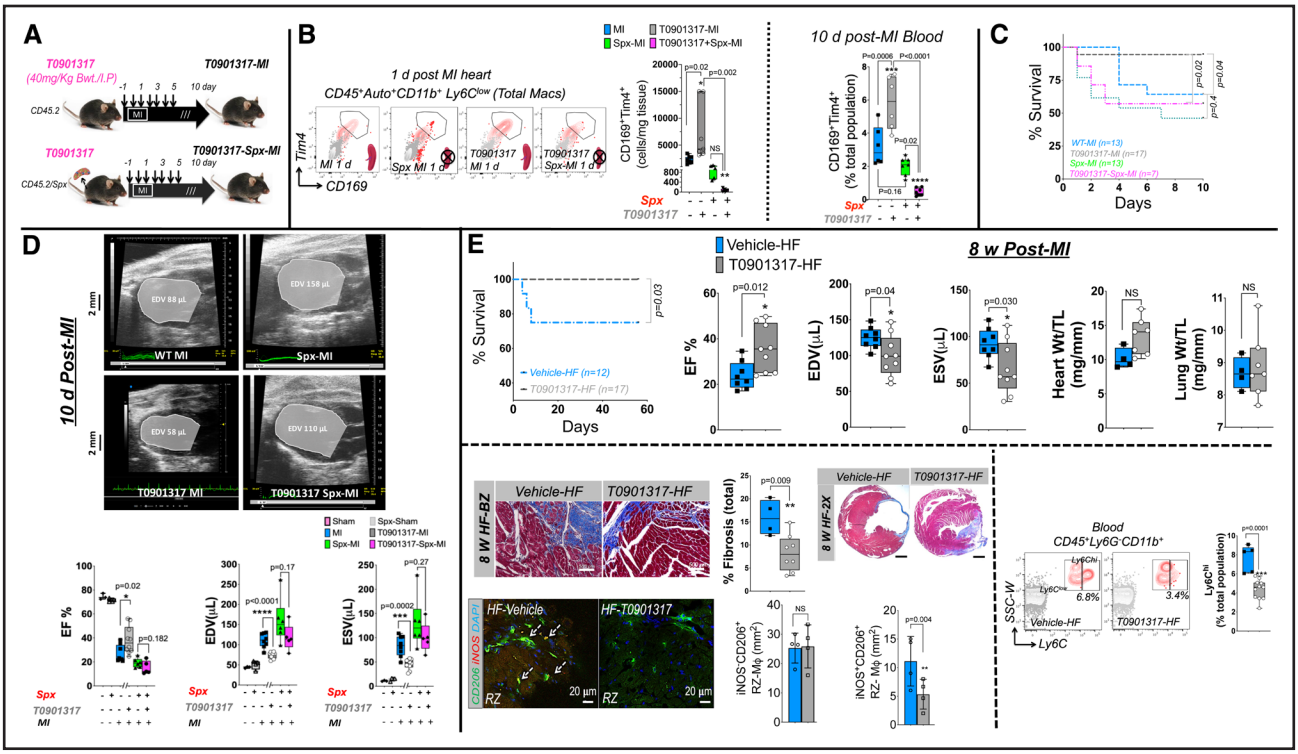

Figure 7. Splenic marginal zone expansion alleviates left ventricular remodeling and inflammation after myocardial infarction. **A**, Protocol for LXRα agonist T0901317 treatment (40 mg/kg IP) from 1 day before to 5 days after myocardial infarction (MI), with 10 days after MI follow-up, in wild-type (WT) and splenectomized mice. **B**, Fluorescence-activated cell sorting contour plots and quantitation of cardiac CD169$^+$Tim4$^+$ (cluster of differentiation 169; T cell immunoglobulin– and mucin-domain–containing molecule 4) macrophages 1 day after MI and blood CD169$^+$Tim4$^+$ monocytes 10 days after MI in untreated and T0901317-treated WT and splenectomized mice (n=5 or 6/group). Welch ANOVA, Dunnett T3 post-test. **C**, Kaplan-Meier survival curves after MI in untreated and T0901317-treated WT and splenectomized mice. Statistical comparisons by log-rank test; group sizes as indicated. **D**, Representative end-diastolic long-axis 2-dimensional echocardiograms and group data for left ventricular (LV) ejection fraction (EF) and end-diastolic volume (EDV) and end-systolic volume (ESV) in the same mouse groups at 10 days after MI or sham operation, as indicated (n=5–10/group). One-way ANOVA, Bonferroni post-test. **E**, **Top**, Kaplan-Meier survival curves over 8 weeks after MI in WT mice treated with either vehicle or T0901317 from 1 day before MI to 5 days after MI (statistical comparison by log-rank test; n=12–17/group, as indicated) and group data for LV EF, EDV, and ESV, and normalized heart and lung weight, at 8 weeks after MI (n=8 or 9/group for echocardiography, n=4–7/group for gravimetry). Unpaired *t* test. Bottom Left, Representative Masson trichrome staining of LV short-axis sections (2× magnification) and infarct border zone (BZ; scale bar=500 µm), along with quantitation of cardiac fibrosis (BZ and remote zone [RZ]; blue staining) in vehicle- and T0901317-treated WT HF mice. Also shown are confocal images of immunofluorescent staining for CD206 (green) and inducible nitric oxide synthase (iNOS; red) in the RZ of hearts from vehicle- and T0901317-treated heart failure (HF) mice (8 weeks after MI) and quantitation of iNOS$^+$CD206$^+$ and iNOS$^-$CD206$^+$ macrophages (Mφ)/mm^2. Double-positive (CD206$^+$iNOS$^+$) cells appear yellow (arrows). DAPI (blue) was used for nuclear staining; n=4–8/group. Unpaired *t* test. **Bottom Right**, Representative fluorescence-activated cell sorting contour plots to identify Ly6C^{hi} (lymphocyte antigen 6 complex, locus C) monocytes in vehicle- and T0901317-treated WT HF mice (8 w after MI), and corresponding quantitation (n=5–10/group). Mann-Whitney *U* test. NS indicates not significant; and TL, tibia length.

proinflammatory iNOS$^+$CD206$^+$ macrophages and circulating Ly6C^{hi} monocytes with T0901317 treatment, but comparable levels of iNOS$^-$CD206$^+$ cardiac macrophages compared with vehicle-treated MI mice (Figure 7E). Taken together, these results establish splenic dependence of the remodeling benefits of the LXRα agonist T0901317 and that MZM expansion is cardioprotective after MI, suppressing cardiac inflammation and improving short- and long-term cardiac remodeling.

Blood CD64+CD169+Tim4+ Monocytes Expand After STEMI in Humans

Blood was collected from patients with acute ST-segment–elevation MI (STEMI) before urgent coronary reperfusion and from controls undergoing elective PCI. The 2 groups were relatively matched for age, sex, and race, and had comparable comorbidity burden, as depicted in Table S4. Using the gating strategy in Figure 8A, we identified human leukocyte antigen–DR (HLA-DR)$^+$CD64$^+$CD169$^+$Tim4$^+$ cells within the circulating CD14$^+$ monocyte population. We performed further validation by sorting and visualizing CD14$^+$HLA-DR$^+$CD169$^+$ monocytes using FACS and imaging flow cytometry (Figure 8B). Robust CD169 expression was readily observed in sorted cells. CD169$^+$ monocytes exhibited a narrower size distribution (≈9 µm) after STEMI compared with controls (8–11 µm; Figure 8B), suggesting an altered activation state. Quantitation by flow cytometry revealed robustly increased frequency

ORIGINAL RESEARCH ARTICLE

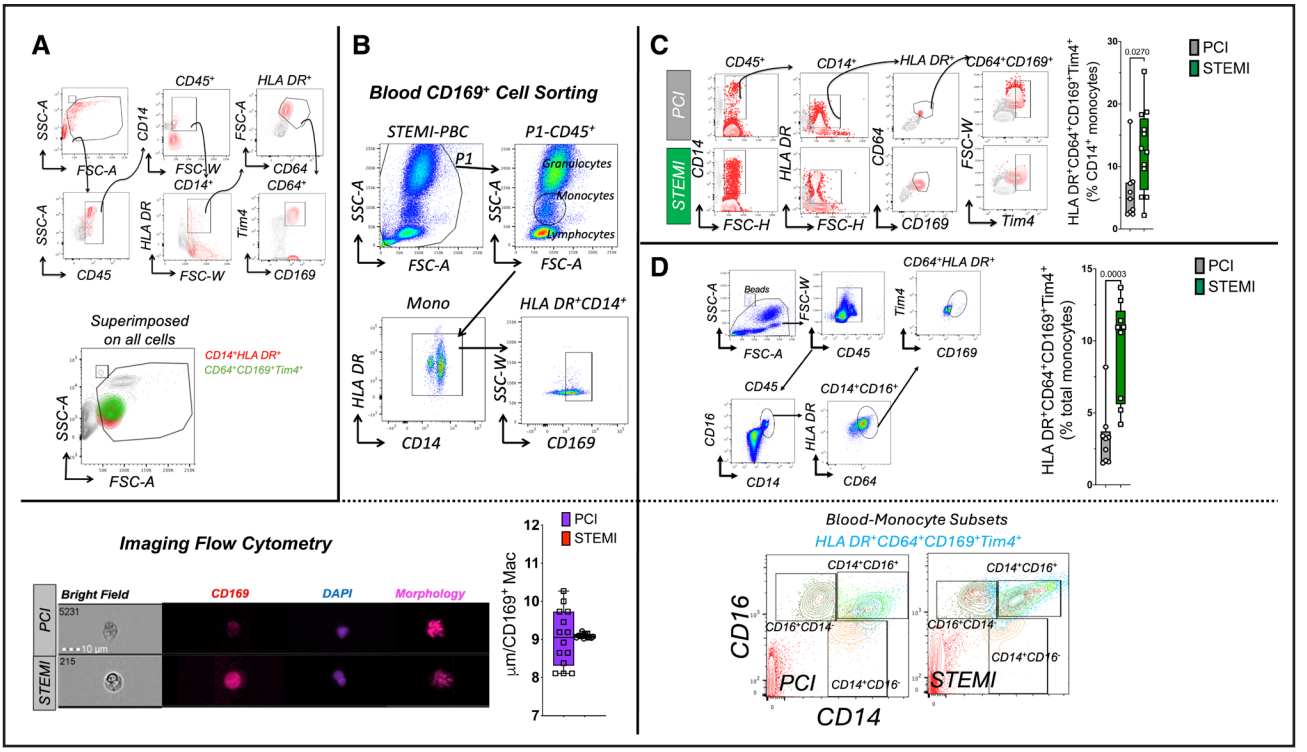

Figure 8. CD169+Tim4+ monocyte expansion after ST-segment–elevation myocardial infarction in humans.
A, Fluorescence-activated cell sorting plots and characterization of human CD45⁺CD14⁺HLA-DR⁺CD64⁺CD169⁺Tim4⁺ (clusters of differentiation 45 and 14; human leukocyte antigen–DR; clusters of differentiation 64 and 169; T cell immunoglobulin– and mucin-domain–containing molecule 4) circulating monocytes from a patient with acute STEMI. The accompanying overlaid contour plot illustrates CD14⁺HLA-DR⁺ (red) and CD64⁺CD169⁺Tim4⁺ (green) subsets superimposed on all CD45⁺ leukocytes in an SSC-A versus FSC-A gate. **B**, **Top**, Fluorescence-activated cell sorting gating strategy for sorting CD45⁺CD14⁺HLA-DR⁺CD169⁺ cells from human peripheral blood for further characterization using ImageStream analysis. **Bottom**, ImageStream visualization of fluorescence-activated cell–sorted CD169⁺ blood cells from patients with STEMI and controls undergoing elective percutaneous coronary intervention (PCI), and group data for size distribution of CD169⁺ cells (n=14/group). Scale bar=10 μm. Fluorescence-activated cell sorting plots and frequency of circulating HLA-DR⁺CD64⁺CD169⁺Tim4⁺ monocytes within CD14⁺ monocytes (**C**) and all blood monocytes (**D**) in STEMI and PCI controls. Also shown in **D** are HLA-DR⁺CD64⁺CD169⁺Tim4⁺ cells (cyan) backgated on monocyte subsets (n=9–12/group): classic (CD14⁺CD16⁻; orange), intermediate (CD14⁺CD16⁺; green), and nonclassic (CD16⁺CD14⁻; gray). Unpaired *t* test.

of circulating HLA-DR⁺CD64⁺CD169⁺Tim4⁺ monocytes within the CD14⁺ monocyte population and within the total monocyte (CD14⁺, CD16⁺, or dual positive) population in patients with STEMI versus PCI controls (Figure 8C and 8D). Backgating revealed that HLA-DR⁺CD64⁺CD169⁺Tim4⁺ cells circulated primarily as intermediate CD14⁺CD16⁺ blood monocytes (Figure 8D). These data suggest mobilization of activated CD169⁺ monocytes after acute MI in humans, analogous to mice.

DISCUSSION

We have established a novel role for splenic CD169⁺Tim4⁺ MMMs, and the cardiosplenic axis, in the inflammatory, healing, and remodeling responses after MI. There are several key findings. First, splenic CD169⁺Tim4⁺ MMMs circulate as a Ly6C^{low} monocyte subpopulation and help maintain CD169⁺Tim4⁺CCR2⁻LYVE1^{low} macrophages in the heart. Second, after acute MI, splenic CD169⁺Tim4⁺ MMMs augment phagocytosis and mobilize to the heart in response to chemotactic signals, resulting in marked expansion of CD169⁺Tim4⁺LYVE1^{low} macrophages with an immunomodulatory and proresolving gene signature. Third, splenic MMMs play a crucial role in efferocytosis after MI, particularly in clearance of apoptotic neutrophils, and are obligatory for inducing a reparative macrophage phenotype. Fourth, splenic CD169⁺Tim4⁺ macrophages are both necessary and sufficient for post-MI wound healing, and limit long-term pathological remodeling. Fifth, LXRα agonist–induced expansion of splenic MZMs alleviates adverse post-MI LV remodeling and inflammation, suggesting a translational approach for splenic modulation. Sixth, humans also exhibit expansion of circulating CD64⁺CD169⁺Tim4⁺ monocytes after acute STEMI. These data collectively establish that splenic CD169⁺Tim4⁺ MMMs traffic to the heart and are required for proresolving and reparative responses after MI. These macrophages limit long-term pathological LV remodeling and can potentially be manipulated for therapeutic benefit.

Interfacing the white and red pulp, the splenic MZ is an important sinusoidal system for the transit of blood leukocytes.[9] It contains specialized CD169$^+$ MMMs that clear apoptotic cells through phagocytic receptors such as Tim4,[13] capture bloodborne antigens, and regulate subsequent adaptive immune responses.[36,37] Expression of CD169, a lectin-like receptor, is restricted to tissue-resident macrophages in various organs. Spatial localization of CD169$^+$ macrophages in close proximity to endothelial cells in the splenic MZ, within hepatic sinusoids, and adjacent to the brain and kidney vasculature suggests that they serve as frontline sentinels in phagocytosing and removing bloodborne particulate antigens.[38,39] MZMs are required for both establishing tolerance to apoptotic cell antigens,[40] an essential step to reduce immunogenicity of autoantigens, as well as amplifying immune responses through interactions with dendritic cells, indicating dual regulation of both tolerogenic and proinflammatory responses.

CD169$^+$ MMMs are classically considered tissue resident at steady-state, dependent on CCL19 and CCL21 for splenic localization.[9,37] However, our data indicate that splenic CD169$^+$Tim4$^+$ macrophages can circulate in blood as Ly6C^{low}CD169$^+$Tim4$^+$ monocytes expressing CD64 and several key macrophage genes, and populate CD169$^+$Tim4$^+$LyVE1^{low} macrophages in the heart. Mobilization of MMMs may relate to their unique anatomic localization, with splenic marginal sinus lining endothelial cells during dynamic movement of blood from the white pulp to the red pulp.[38] Indeed, the circulating cells exhibited projections reminiscent of splenic MMM processes that penetrate the white pulp.[37] Moreover, splenectomy induced an ≈80% loss of cardiac CD169$^+$Tim4$^+$ macrophages and ≈70% loss of circulating Ly6C^{low}CD169$^+$Tim4$^+$ monocytes, consistent with an active splenocardiac MMM circulation. CD169$^+$Tim4$^+$ macrophages are particularly important as an immunoregulatory and hypostimulatory tissue-resident macrophage subset.[16] Whereas both splenectomy and CD169 ablation significantly reduced total Ly6C^{low} monocytes, neither affected levels of proinflammatory Ly6C^{hi} monocytes.

Given a steady-state splenocardiac circulation of CD169$^+$Tim4$^+$ macrophages, the recognized rapid turnover of splenic MMMs during inflammatory states,[37,41] and their importance in immunoregulation,[16] we explored their role in acute MI. It is established that splenic subcapsular red pulp reservoir Ly6C^{hi} monocytes infiltrate the heart and contribute to both inflammation and repair after acute MI.[2–5,8,37,41] Here we show, for the first time to our knowledge, that Ly6C^{low}CD169$^+$Tim4$^+$ splenic MMMs also robustly mobilize to the heart after acute MI, as splenectomy dramatically reduced the cardiac recruitment of CD169$^+$Tim4$^+$LYVE1^{low} macrophages, and also resulted in augmented donor splenic MMM recruitment in parabiotic models. CD169$^+$Tim4$^+$ monocytes exhibited increased surface expression of CCR3 and CCR4 in conjunction with upregulation of several corresponding chemokine ligands in the infarcted heart. Spleen-derived MMMs augmented phagocytic capacity after MI, suggesting that efferocytosis is a key role for these cells.

CD169$^+$Tim4$^+$ MMMs were proresolving, anti-inflammatory, and reparative in the infarcted heart. One mechanism underlying these effects may be their impact on neutrophil clearance and production. Tim4 binds phosphatidylserine residues on the surface of apoptotic cells, allowing for engulfment and prevention of ambient release of toxic materials from dead cells.[13] Acutely after MI, there is intense neutrophil infiltration for removal of tissue debris.[1,5] Neutrophils have short life spans and undergo apoptosis,[42] necessitating their efferocytosis in the acutely infarcted heart. Our studies with Catchup mice established that CD169$^+$Tim4$^+$ macrophages take up apoptotic neutrophils, whereas MMM loss upon either splenectomy or CD169 ablation significantly increased the number of apoptotic neutrophils in the infarcted heart. Apoptotic neutrophil levels normalized upon adoptive transfer of splenic CD169$^+$Tim4$^+$ MMMs in splenectomized MI mice, establishing these cells as crucial mediators of neutrophil efferocytosis after MI.

Apoptotic neutrophil disposal triggers anti-inflammatory and immunosuppressive signals in engulfing phagocytes,[43] including an IL-12^{low}IL-10^{high} regulatory phenotype[44] that promotes tissue repair. In our studies, mice with MMM deficiency after splenectomy or CD169 ablation exhibited significantly fewer cardiac Ly6C^{low} cells expressing anti-inflammatory IL-10 or IL-4 24 hours after MI, more pronounced proinflammatory Ly6C^{hi} monocytosis and lower anti-inflammatory serum IL-10 levels at 10 days after MI, and persistence of proinflammatory iNOS$^+$CD206$^+$ macrophages at later stages (10 days and 8 weeks) after MI. Proinflammatory macrophage abundance, Ly6C^{hi} monocytosis, and serum IL-10 levels were all normalized upon adoptive transfer of splenic CD169$^+$Tim4$^+$ MMMs in splenectomized MI mice. Hence, whereas the impact of the spleen on the heart likely relates to multiple cell types, these studies establish that splenic MMMs are essential for the development of a proresolving program in cardiac macrophages after MI.

Loss of splenic Ly6C^{low}CD169$^+$Tim4$^+$ cells also augmented neutrophil activity and accumulation in the heart, thereby sustaining tissue inflammation. Both splenectomized and CD169 ablated mice exhibited increased total and ICAM1$^+$ (intercellular adhesion molecule 1) activated blood neutrophils, myocardial neutrophils, and bone marrow granulocyte-macrophage progenitors (suggesting greater granulopoiesis) acutely (24 hours) after MI. Although not examined specifically, extramedullary granulopoiesis may have been similarly affected. Bone marrow and myocardial neutrophils were markedly suppressed upon splenic CD169$^+$Tim4$^+$ MMM adoptive transfer in splenectomized MI mice. These data are consistent with previous work showing that Ly6C^{low}CD169$^+$ macrophages limit

kidney accumulation and injury after ischemia-reperfusion by suppressing vascular endothelial ICAM-1 expression[45]; mice deficient in MZ and bone marrow stromal cell macrophages resulting from myeloid C-FLIP (cellular FLICE-like inhibitory protein) deficiency exhibit excess G-CSF (granulocyte colony-stimulating factor)–driven granulopoiesis because of the failure of macrophages to efficiently clear apoptotic neutrophils[46]; and acute CD169$^+$ macrophage depletion significantly expands an activated aged neutrophil subset.[47] Hence, the anti-inflammatory and reparative effects of splenic CD169$^+$Tim4$^+$ MMMs appear tightly linked to neutrophil responses.

In concert with immunomodulatory effects, CD169$^+$Tim4$^+$ MMMs induced functional benefits in the infarcted heart, promoting cardiac wound healing and limiting early and late LV remodeling and dysfunction. Both splenectomized and CD169 ablated MI mice exhibited higher 10-day mortality after MI because of increased cardiac rupture, indicative of impaired wound healing. Lower survival was accompanied by lower matrix metalloproteinase-9 levels and reduced border zone fibrosis at 10 days after MI, indicating diminished extracellular matrix turnover and healing scar formation, together with increased LV chamber dilatation and systolic dysfunction. CD169$^+$Tim4$^+$ MMM adoptive transfer in splenectomized MI mice improved survival, prevented rupture, restored border zone matrix metalloproteinase-9 and fibrosis, and alleviated LV dilatation at 10 days after MI. The long-term remodeling effects (8 weeks after MI) of splenic MMM deficiency included thinner scars and increased LV dilatation, systolic dysfunction, hypertrophy, and lung edema. These data indicate that splenic CD169$^+$Tim4$^+$ MMMs are obligatory for optimal post-MI wound healing to limit the late development of ischemic cardiomyopathy.

It is known that splenectomized mice exhibit exaggerated early LV remodeling after MI.[8] Our results establish that this impaired healing is in part dependent on the loss of splenic CD169$^+$ MMMs. More recent work demonstrated that CD169$^+$ macrophage depletion 1 week before reperfused MI worsened post-MI remodeling.[24] In that study, CD169 was used as a marker of tissue resident macrophages to understand the impact of cardiac CCR2$^-$ cells. Our results indicate that detrimental effects of CD169$^+$ macrophage ablation are also attributable to the loss of splenic MMMs, as nonsplenic derived cardiac resident CD169$^+$Tim4$^+$ cells would not be affected by splenectomy. The prohealing effects of the spleen on the heart during acute MI described here contrasts with the detrimental cardiosplenic axis in chronic ischemic HF that we have described previously.[48] This suggests a pathological change in the splenic immune cell milieu in chronic HF that favors tissue injury rather than healing, and carries important translational implications for wound healing after a first MI versus recurrent MI in the context of chronic HF.

The previous studies established the necessity of splenic MMMs for post-MI wound healing. We also wanted to establish whether expansion of splenic MMMs would improve endogenous repair. LXRs are nuclear receptors that are key transcriptional regulators of metabolic and immune responses in macrophages, including the phagocytic clearance of apoptotic cells and immune tolerance.[34,49] Among the LXRα and LXRβ isoforms, LXRα is specifically required for the development and generation of MMMs (and MZMs).[50] LXRα-deficient mice exhibit selective loss of MZMs, without affecting CD169$^+$ macrophage populations in other tissues.[50] Moreover, LXRα activation accelerates MZM development and expansion. Therefore, we used pharmacological LXRα agonism to expand splenic MMMs and their efferocytotic capacity to evaluate therapeutic benefit of MMM gain of function after MI. Because LXRs are expressed in several tissues, we isolated the splenic effects of LXRα agonism by comparing responses in WT and splenectomized mice. Pharmacological LXRα augmentation with T0901317 robustly increased splenic and circulating CD169$^+$Tim4$^+$ cells at steady state and splenic CD169$^+$Tim4$^+$ MMM infiltration in the acutely infarcted heart. T0901317 improved 10-day post-MI survival and LV remodeling in WT mice, but not in splenectomized mice, indicating splenic dependence of these effects. Long-term effects included alleviation of late LV systolic dysfunction, total fibrosis, and reduction of proinflammatory monocytes and macrophages, suggesting chronic suppression of local and systemic inflammation.

LXRα agonism may be a potential translational approach to favorably modulate the spleen after MI. Both dual LXRα/β agonists[51] and LXRα-selective agonists[52] protect against adverse LV remodeling from pressure overload, whereas such remodeling is worsened in LXRα-null mice.[51] Bolstering the case for clinical relevance, analogous to mice with acute MI, humans with acute STEMI also exhibited marked expansion of circulating CD64$^+$CD169$^+$Tim4$^+$ intermediate monocytes, along with size distribution characteristics suggesting an altered activation state, compared with control PCI participants matched for age, sex, race, and comorbidities. Whereas the source of these CD169$^+$ cells was not definitively determined, previous work has indicated that patients with acute coronary syndrome have increased splenic metabolic activity, as measured by ^{18}F-fluorodeoxyglucose–positron emission tomography, which correlates with proinflammatory remodeling of blood leukocytes and the risk of subsequent cardiovascular events.[53] Hence, acute activation of the cardiosplenic axis after MI in humans may well include activation and mobilization of CD169$^+$ MMMs to the infarct to participate in MI healing. Of note, CD169$^+$ blood monocytes have been observed in humans with gastrointestinal malignancies, metastatic melanoma, and COVID-19, and were suggested to represent a heightened monocyte activation state.[54] Moreover, splenectomy in humans has been reported as increasing

the long-term risk of cardiac ischemic events and MI.[55] However, it is not clear whether splenectomy augments the risk of adverse post-MI remodeling in humans. Further studies will be required to further delineate this phenomenon and its implications for post-MI prognosis and outcomes.

Conclusions

Splenic CD169$^+$Tim4$^+$ MMMs play a central role in the healing and repair response after MI. They comprise a key cellular component of the cardiosplenic axis both at baseline and after acute myocardial injury. Splenic MMMs play a crucial role in dead cell clearance, particularly of apoptotic neutrophils; induction of reparative tissue macrophages; inflammation resolution; and proper wound healing after MI. Expansion of the splenic MZ improves the LV remodeling response and alleviates inflammation, raising the possibility of splenic modulation as a therapeutic intervention during the acute MI period to prevent the late development of HF.

ARTICLE INFORMATION

Received August 8, 2024; accepted March 31, 2025.

Affiliations

Division of Cardiology, Department of Medicine, Washington University in St Louis, MO (M.A.I., S.R., G.R., T.H., S.D.P.). Departments of Medicine, Cardiovascular Disease (M.A.I., G.Z., M.G., S.S.B., B.P., M.X., S.A., G.R., T.H., S.D.P.), and Neurology (N.L.), University of Alabama at Birmingham. Dr Bansal is currently affiliated with the Heart and Vascular Institute, Department of Medicine, Milton S. Hershey Medical Center, Pennsylvania State University, Hershey.

Acknowledgments

The authors thank the Genome Technology Access Center, McDonnell Genome Institute, Washington University School of Medicine, for help with genomic analysis.

Sources of Funding

This work was supported by National Institutes of Health grants R01 HL125735 and R01 HL157999 (Dr Prabhu), K24 HL133373 (Dr Limdi), R03 HL141620 (Dr Xie), and R01 HL137046 (Dr Hamid); and Veterans Affairs grant I01 BX002706 (Dr Prabhu).

Disclosures

None.

Supplemental Material

Methods
Tables S1–S5
Figures S1–S13
References 56–75

REFERENCES

1. Prabhu SD, Frangogiannis NG. The biological basis for cardiac repair after myocardial infarction: from inflammation to fibrosis. *Circ Res*. 2016;119:91–112. doi: 10.1161/CIRCRESAHA.116.303577
2. Hilgendorf I, Gerhardt LM, Tan TC, Winter C, Holderried TA, Chousterman BG, Iwamoto Y, Liao R, Zirlik A, Scherer-Crosbie M, et al. Ly-6C^{high} monocytes depend on Nr4a1 to balance both inflammatory and reparative phases in the infarcted myocardium. *Circ Res*. 2014;114:1611–1622. doi: 10.1161/CIRCRESAHA.114.303204
3. Leuschner F, Dutta P, Gorbatov R, Novobrantseva TI, Donahoe JS, Courties G, Lee KM, Kim JI, Markmann JF, Marinelli B, et al. Therapeutic siRNA silencing in inflammatory monocytes in mice. *Nat Biotechnol*. 2011;29:1005–1010. doi: 10.1038/nbt.1989
4. Swirski FK, Nahrendorf M, Etzrodt M, Wildgruber M, Cortez-Retamozo V, Panizzi P, Figueiredo JL, Kohler RH, Chudnovskiy A, Waterman P, et al. Identification of splenic reservoir monocytes and their deployment to inflammatory sites. *Science*. 2009;325:612–616. doi: 10.1126/science.1175202
5. Yan X, Anzai A, Katsumata Y, Matsuhashi T, Ito K, Endo J, Yamamoto T, Takeshima A, Shinmura K, Shen W, et al. Temporal dynamics of cardiac immune cell accumulation following acute myocardial infarction. *J Mol Cell Cardiol*. 2013;62:24–35. doi: 10.1016/j.yjmcc.2013.04.023
6. Horckmans M, Ring L, Duchene J, Santovito D, Schloss MJ, Drechsler M, Weber C, Soehnlein O, Steffens S. Neutrophils orchestrate post-myocardial infarction healing by polarizing macrophages towards a reparative phenotype. *Eur Heart J*. 2017;38:187–197. doi: 10.1093/eurheartj/ehw002
7. Wan E, Yeap XY, Dehn S, Terry R, Novak M, Zhang S, Iwata S, Han X, Homma S, Drosatos K, et al. Enhanced efferocytosis of apoptotic cardiomyocytes through myeloid-epithelial-reproductive tyrosine kinase links acute inflammation resolution to cardiac repair after infarction. *Circ Res*. 2013;113:1004–1012. doi: 10.1161/CIRCRESAHA.113.301198
8. Leuschner F, Rauch PJ, Ueno T, Gorbatov R, Marinelli B, Lee WW, Dutta P, Wei Y, Robbins C, Iwamoto Y, et al. Rapid monocyte kinetics in acute myocardial infarction are sustained by extramedullary monocytopoiesis. *J Exp Med*. 2012;209:123–137. doi: 10.1084/jem.20111009
9. Mebius RE, Kraal G. Structure and function of the spleen. *Nat Rev Immunol*. 2005;5:606–616. doi: 10.1038/nri1669
10. Taylor PR, Martinez-Pomares L, Stacey M, Lin HH, Brown GD, Gordon S. Macrophage receptors and immune recognition. *Annu Rev Immunol*. 2005;23:901–944. doi: 10.1146/annurev.immunol.23.021704.115816
11. Miyake Y, Asano K, Kaise H, Uemura M, Nakayama M, Tanaka M. Critical role of macrophages in the marginal zone in the suppression of immune responses to apoptotic cell-associated antigens. *J Clin Invest*. 2007;117:2268–2278. doi: 10.1172/JCI31990
12. O'Neill AS, van den Berg TK, Mullen GE. Sialoadhesin: a macrophage-restricted marker of immunoregulation and inflammation. *Immunology*. 2013;138:198–207. doi: 10.1111/imm.12042
13. Miyanishi M, Tada K, Koike M, Uchiyama Y, Kitamura T, Nagata S. Identification of Tim4 as a phosphatidylserine receptor. *Nature*. 2007;450:435–439. doi: 10.1038/nature06307
14. Dick SA, Macklin JA, Nejat S, Momen A, Clemente-Casares X, Althagafi MG, Chen J, Kantores C, Hosseinzadeh S, Aronoff L, et al. Self-renewing resident cardiac macrophages limit adverse remodeling following myocardial infarction. *Nat Immunol*. 2019;20:29–39. doi: 10.1038/s41590-018-0272-2
15. Revelo XS, Parthiban P, Chen C, Barrow F, Fredrickson G, Wang H, Yucel D, Herman A, van Berlo JH. Cardiac resident macrophages prevent fibrosis and stimulate angiogenesis. *Circ Res*. 2021;129:1086–1101. doi: 10.1161/CIRCRESAHA.121.319737
16. Thornley TB, Fang Z, Balasubramanian S, Larocca RA, Gong W, Gupta S, Csizmadia E, Degauque N, Kim BS, Koulmanda M, et al. Fragile TIM-4-expressing tissue resident macrophages are migratory and immunoregulatory. *J Clin Invest*. 2014;124:3443–3454. doi: 10.1172/JCI73527
17. Cavasin MA, Tao Z, Menon S, Yang XP. Gender differences in cardiac function during early remodeling after acute myocardial infarction in mice. *Life Sci*. 2004;75:2181–2192. doi: 10.1016/j.lfs.2004.04.024
18. Pullen AB, Kain V, Serhan CN, Halade GV. Molecular and cellular differences in cardiac repair of male and female mice. *J Am Heart Assoc*. 2020;9:e015672. doi: 10.1161/JAHA.119.015672
19. Gautier EL, Shay T, Miller J, Greter M, Jakubzick C, Ivanov S, Helft J, Chow A, Elpek KG, Gordonov S, et al; Immunological Genome Consortium. Gene-expression profiles and transcriptional regulatory pathways that underlie the identity and diversity of mouse tissue macrophages. *Nat Immunol*. 2012;13:1118–1128. doi: 10.1038/ni.2419
20. Tamoutounour S, Henri S, Lelouard H, de Bovis B, de Haar C, van der Woude CJ, Woltman AM, Reyal Y, Bonnet D, Sichien D, et al. CD64 distinguishes macrophages from dendritic cells in the gut and reveals the Th1-inducing role of mesenteric lymph node macrophages during colitis. *Eur J Immunol*. 2012;42:3150–3166. doi: 10.1002/eji.201242847
21. Wong A, Hamidzada H, Epelman S. A cardioimmunologist's toolkit: genetic tools to dissect immune cells in cardiac disease. *Nat Rev Cardiol*. 2022;19:395–413. doi: 10.1038/s41569-022-00701-0
22. Sager HB, Hulsmans M, Lavine KJ, Moreira MB, Heidt T, Courties G, Sun Y, Iwamoto Y, Tricot B, Khan OF, et al. Proliferation and recruitment contribute to myocardial macrophage expansion in chronic heart failure. *Circ Res*. 2016;119:853–864. doi: 10.1161/CIRCRESAHA.116.309001

23. Pinto AR, Paolicelli R, Salimova E, Gospocic J, Slonimsky E, Bilbao-Cortes D, Godwin JW, Rosenthal NA. An abundant tissue macrophage population in the adult murine heart with a distinct alternatively-activated macrophage profile. *PLoS One*. 2012;7:e36814. doi: 10.1371/journal.pone.0036814
24. Bajpai G, Bredemeyer A, Li W, Zaitsev K, Koenig AL, Lokshina I, Mohan J, Ivey B, Hsiao HM, Weinheimer C, et al. Tissue resident CCR2- and CCR2+ cardiac macrophages differentially orchestrate monocyte recruitment and fate specification following myocardial injury. *Circ Res*. 2019;124:263–278. doi: 10.1161/CIRCRESAHA.118.314028
25. Aran D, Looney AP, Liu L, Wu E, Fong V, Hsu A, Chak S, Naikawadi RP, Wolters PJ, Abate AR, et al. Reference-based analysis of lung single-cell sequencing reveals a transitional profibrotic macrophage. *Nat Immunol*. 2019;20:163–172. doi: 10.1038/s41590-018-0276-y
26. Krasniewski LK, Chakraborty P, Cui CY, Mazan-Mamczarz K, Dunn C, Piao Y, Fan J, Shi C, Wallace T, Nguyen C, et al. Single-cell analysis of skeletal muscle macrophages reveals age-associated functional subpopulations. *Elife*. 2022;11:e77974. doi: 10.7554/eLife.77974
27. Wauters E, Van Mol P, Garg AD, Jansen S, Van Herck Y, Vanderbeke L, Bassez A, Boeckx B, Malengier-Devlies B, Timmerman A, et al; CONTAGIOUS collaborators. Discriminating mild from critical COVID-19 by innate and adaptive immune single-cell profiling of bronchoalveolar lavages. *Cell Res*. 2021;31:272–290. doi: 10.1038/s41422-020-00455-9
28. Griffith JW, Sokol CL, Luster AD. Chemokines and chemokine receptors: positioning cells for host defense and immunity. *Annu Rev Immunol*. 2014;32:659–702. doi: 10.1146/annurev-immunol-032713-120145
29. Voll RE, Herrmann M, Roth EA, Stach C, Kalden JR, Girkontaite I. Immunosuppressive effects of apoptotic cells. *Nature*. 1997;390:350–351. doi: 10.1038/37022
30. McDonald PP, Fadok VA, Bratton D, Henson PM. Transcriptional and translational regulation of inflammatory mediator production by endogenous TGF-beta in macrophages that have ingested apoptotic cells. *J Immunol*. 1999;163:6164–6172.
31. Hasenberg A, Hasenberg M, Mann L, Neumann F, Borkenstein L, Stecher M, Kraus A, Engel DR, Klingberg A, Seddigh P, et al. Catchup: a mouse model for imaging-based tracking and modulation of neutrophil granulocytes. *Nat Methods*. 2015;12:445–452. doi: 10.1038/nmeth.3322
32. Shiraishi M, Shintani Y, Shintani Y, Ishida H, Saba R, Yamaguchi A, Adachi H, Yashiro K, Suzuki K. Alternatively activated macrophages determine repair of the infarcted adult murine heart. *J Clin Invest*. 2016;126:2151–2166. doi: 10.1172/JCI85782
33. Rebe C, Raveneau M, Chevriaux A, Lakomy D, Sberna AL, Costa A, Bessede G, Athias A, Steinmetz E, Lobaccaro JM, et al. Induction of transglutaminase 2 by a liver X receptor/retinoic acid receptor alpha pathway increases the clearance of apoptotic cells by human macrophages. *Circ Res*. 2009;105:393–401. doi: 10.1161/CIRCRESAHA.109.201855
34. Alonso-Gonzalez N, Bensinger SJ, Hong C, Beceiro S, Bradley MN, Zelcer N, Deniz J, Ramirez C, Diaz M, Gallardo G, et al. Apoptotic cells promote their own clearance and immune tolerance through activation of the nuclear receptor LXR. *Immunity*. 2009;31:245–258. doi: 10.1016/j.immuni.2009.06.018
35. Schultz JR, Tu H, Luk A, Repa JJ, Medina JC, Li L, Schwendner S, Wang S, Thoolen M, Mangelsdorf DJ, et al. Role of LXRs in control of lipogenesis. *Genes Dev*. 2000;14:2831–2838. doi: 10.1101/gad.850400
36. Davies LC, Jenkins SJ, Allen JE, Taylor PR. Tissue-resident macrophages. *Nat Immunol*. 2013;14:986–995. doi: 10.1038/ni.2705
37. Lewis SM, Williams A, Eisenbarth SC. Structure and function of the immune system in the spleen. *Sci Immunol*. 2019;4:eaau6085. doi: 10.1126/sciimmunol.aau6085
38. Alonso-Gonzalez N, Castrillo A. Origin and specialization of splenic macrophages. *Cell Immunol*. 2018;330:151–158. doi: 10.1016/j.cellimm.2018.05.005
39. Gupta P, Lai SM, Sheng J, Tetlak P, Balachander A, Claser C, Renia L, Karjalainen K, Ruedl C. Tissue-resident CD169(+) macrophages form a crucial front line against plasmodium infection. *Cell Rep*. 2016;16:1749–1761. doi: 10.1016/j.celrep.2016.07.010
40. McGaha TL, Chen Y, Ravishankar B, van Rooijen N, Karlsson MC. Marginal zone macrophages suppress innate and adaptive immunity to apoptotic cells in the spleen. *Blood*. 2011;117:5403–5412. doi: 10.1182/blood-2010-11-320028
41. Bronte V, Pittet MJ. The spleen in local and systemic regulation of immunity. *Immunity*. 2013;39:806–818. doi: 10.1016/j.immuni.2013.10.010
42. Geering B, Stoeckle C, Conus S, Simon HU. Living and dying for inflammation: neutrophils, eosinophils, basophils. *Trends Immunol*. 2013;34:398–409. doi: 10.1016/j.it.2013.04.002
43. Fox S, Leitch AE, Duffin R, Haslett C, Rossi AG. Neutrophil apoptosis: relevance to the innate immune response and inflammatory disease. *J Innate Immun*. 2010;2:216–227. doi: 10.1159/000284367
44. Filardy AA, Pires DR, Nunes MP, Takiya CM, Freire-de-Lima CG, Ribeiro-Gomes FL, DosReis GA. Proinflammatory clearance of apoptotic neutrophils induces an IL-12(low)IL-10(high) regulatory phenotype in macrophages. *J Immunol*. 2010;185:2044–2050. doi: 10.4049/jimmunol.1000017
45. Karasawa K, Asano K, Moriyama S, Ushiki M, Monya M, Iida M, Kuboki E, Yagita H, Uchida K, Nitta K, et al. Vascular-resident CD169-positive monocytes and macrophages control neutrophil accumulation in the kidney with ischemia-reperfusion injury. *J Am Soc Nephrol*. 2015;26:896–906. doi: 10.1681/ASN.2014020195
46. Gordy C, Pua H, Sempowski GD, He YW. Regulation of steady-state neutrophil homeostasis by macrophages. *Blood*. 2011;117:618–629. doi: 10.1182/blood-2010-01-265959
47. Zhang D, Chen G, Manwani D, Mortha A, Xu C, Faith JJ, Burk RD, Kunisaki Y, Jang JE, Scheiermann C, et al. Neutrophil ageing is regulated by the microbiome. *Nature*. 2015;525:528–532. doi: 10.1038/nature15367
48. Ismahil MA, Hamid T, Bansal SS, Patel B, Kingery JR, Prabhu SD. Remodeling of the mononuclear phagocyte network underlies chronic inflammation and disease progression in heart failure: critical importance of the cardiosplenic axis. *Circ Res*. 2014;114:266–282. doi: 10.1161/CIRCRESAHA.113.301720
49. Alonso-Gonzalez N, Castrillo A. Liver X receptors as regulators of macrophage inflammatory and metabolic pathways. *Biochim Biophys Acta*. 2011;1812:982–994. doi: 10.1016/j.bbadis.2010.12.015
50. Alonso-Gonzalez N, Guillen JA, Gallardo G, Diaz M, de la Rosa JV, Hernandez IH, Casanova-Acebes M, Lopez F, Tabraue C, Beceiro S, et al. The nuclear receptor LXRalpha controls the functional specialization of splenic macrophages. *Nat Immunol*. 2013;14:831–839. doi: 10.1038/ni.2622
51. Wu S, Yin R, Ernest R, Li Y, Zhelyabovska O, Luo J, Yang Y, Yang Q. Liver X receptors are negative regulators of cardiac hypertrophy via suppressing NF-kappaB signalling. *Cardiovasc Res*. 2009;84:119–126. doi: 10.1093/cvr/cvp180
52. Kuipers I, Li J, Vreeswijk-Baudoin I, Koster J, van der Harst P, Sillje HH, Kuipers F, van Veldhuisen DJ, van Gilst WH, de Boer RA. Activation of liver X receptors with T0901317 attenuates cardiac hypertrophy in vivo. *Eur J Heart Fail*. 2010;12:1042–1050. doi: 10.1093/eurjhf/hfq109
53. Emami H, Singh P, MacNabb M, Vucic E, Lavender Z, Rudd JH, Fayad ZA, Lehrer-Graiwer J, Korsgren M, Figueroa AL, et al. Splenic metabolic activity predicts risk of future cardiovascular events: demonstration of a cardiosplenic axis in humans. *JACC Cardiovasc Imaging*. 2015;8:121–130. doi: 10.1016/j.jcmg.2014.10.009
54. Affandi AJ, Olesek K, Grabowska J, Nijen Twilhaar MK, Rodriguez E, Saris A, Zwart ES, Nossent EJ, Kalay H, de Kok M, et al. CD169 defines activated CD14(+) monocytes with enhanced CD8(+) T cell activation capacity. *Front Immunol*. 2021;12:697840. doi: 10.3389/fimmu.2021.697840
55. Schilling RF. Risks and benefits of splenectomy versus no splenectomy for hereditary spherocytosis: a personal view. *Br J Haematol*. 2009;145:728–732. doi: 10.1111/j.1365-2141.2009.07694.x
56. Burnett SH, Kershen EJ, Zhang J, Zeng L, Straley SC, Kaplan AM, Cohen DA. Conditional macrophage ablation in transgenic mice expressing a Fas-based suicide gene. *J Leukoc Biol*. 2004;75:612–623. doi: 10.1189/jlb.0903442
57. Parkhurst CN, Yang G, Ninan I, Savas JN, Yates JR 3rd, Lafaille JJ, Hempstead BL, Littman DR, Gan WB. Microglia promote learning-dependent synapse formation through brain-derived neurotrophic factor. *Cell*. 2013;155:1596–1609. doi: 10.1016/j.cell.2013.11.030
58. Saito M, Iwawaki T, Taya C, Yonekawa H, Noda M, Inui Y, Mekada E, Kimata Y, Tsuru A, Kohno K. Diphtheria toxin receptor-mediated conditional and targeted cell ablation in transgenic mice. *Nat Biotechnol*. 2001;19:746–750. doi: 10.1038/90795
59. Hasenberg A, Hasenberg M, Mann L, Neumann F, Borkenstein L, Stecher M, Kraus A, Engel DR, Klingberg A, Seddigh P, et al. Catchup: a mouse model for imaging-based tracking and modulation of neutrophil granulocytes. *Nat Methods*. 2015;12:445–452. doi: 10.1038/nmeth.3322
60. Cavasin MA, Tao Z, Menon S, Yang XP. Gender differences in cardiac function during early remodeling after acute myocardial infarction in mice. *Life Sci*. 2004;75:2181–2192. doi: 10.1016/j.lfs.2004.04.024
61. Pullen AB, Kain V, Serhan CN, Halade GV. Molecular and cellular differences in cardiac repair of male and female mice. *J Am Heart Assoc*. 2020;9:e015672. doi: 10.1161/JAHA.119.015672

62. Hamid T, Gu Y, Ortines RV, Bhattacharya C, Wang G, Xuan YT, Prabhu SD. Divergent tumor necrosis factor receptor-related remodeling responses in heart failure: role of nuclear factor-kappaB and inflammatory activation. *Circulation*. 2009;119:1386–1397. doi: 10.1161/CIRCULATIONAHA.108.802918
63. Patel B, Ismahil MA, Hamid T, Bansal SS, Prabhu SD. Mononuclear phagocytes are dispensable for cardiac remodeling in established pressure-overload heart failure. *PLoS One*. 2017;12:e0170781. doi: 10.1371/journal.pone.0170781
64. Kamran P, Sereti KI, Zhao P, Ali SR, Weissman IL, Ardehali R. Parabiosis in mice: a detailed protocol. *J Vis Exp*. 2013;80:50556. doi: 10.3791/50556
65. Bansal SS, Ismahil MA, Goel M, Zhou G, Rokosh G, Hamid T, Prabhu SD. Dysfunctional and proinflammatory regulatory T-lymphocytes are essential for adverse cardiac remodeling in ischemic cardiomyopathy. *Circulation*. 2019;139:206–221. doi: 10.1161/CIRCULATIONAHA.118.036065
66. Birjandi SZ, Ippolito JA, Ramadorai AK, Witte PL. Alterations in marginal zone macrophages and marginal zone B cells in old mice. *J Immunol*. 2011;186:3441–3451. doi: 10.4049/jimmunol.1001271
67. Li H, Fu YX, Wu Q, Zhou Y, Crossman DK, Yang P, Li J, Luo B, Morel LM, Kabarowski JH, et al. Interferon-induced mechanosensing defects impede apoptotic cell clearance in lupus. *J Clin Invest*. 2015;125:2877–2890. doi: 10.1172/JCI81059
68. Akashi K, Traver D, Miyamoto T, Weissman IL. A clonogenic common myeloid progenitor that gives rise to all myeloid lineages. *Nature*. 2000;404:193–197. doi: 10.1038/35004599
69. Bansal SS, Ismahil MA, Goel M, Patel B, Hamid T, Rokosh G, Prabhu SD. Activated T lymphocytes are essential drivers of pathological remodeling in ischemic heart failure. *Circ Heart Fail*. 2017;10:e003688. doi: 10.1161/CIRCHEARTFAILURE.116.003688
70. Dobin A, Davis CA, Schlesinger F, Drenkow J, Zaleski C, Jha S, Batut P, Chaisson M, Gingeras TR. STAR: ultrafast universal RNA-seq aligner. *Bioinformatics*. 2013;29:15–21. doi: 10.1093/bioinformatics/bts635
71. Love MI, Huber W, Anders S. Moderated estimation of fold change and dispersion for RNA-seq data with DESeq2. *Genome Biol*. 2014;15:550. doi: 10.1186/s13059-014-0550-8
72. Wolf FA, Angerer P, Theis FJ. SCANPY: large-scale single-cell gene expression data analysis. *Genome Biol*. 2018;19:15. doi: 10.1186/s13059-017-1382-0
73. Franzén O, Gan LM, Bjorkegren JLM. PanglaoDB: a web server for exploration of mouse and human single-cell RNA sequencing data. *Database*. 2019;2019:baz046. doi: 10.1093/database/baz046
74. Meng FL, Huang XL, Qin WY, Liu KB, Wang Y, Li M, Ren YH, Li YZ, Sun YM. singleCellBase: a high-quality manually curated database of cell markers for single cell annotation across multiple species. *Biomark Res*. 2023;11:83. doi: 10.1186/s40364-023-00523-3
75. Hu C, Li T, Xu Y, Zhang X, Li F, Bai J, Chen J, Jiang W, Yang K, Ou Q, et al. CellMarker 2.0: an updated database of manually curated cell markers in human/mouse and web tools based on scRNA-seq data. *Nucleic Acids Res*. 2023;51:D870–D876. doi: 10.1093/nar/gkac947